



HAL
open science

Aceclofenac and interactions analysis in the crystal and COX protein active site

Christian Jelsch, Rajendran Niranjana Devi, Bruce Noll, Benoît Guillot, Israel Samuel, Emmanuel Aubert

► **To cite this version:**

Christian Jelsch, Rajendran Niranjana Devi, Bruce Noll, Benoît Guillot, Israel Samuel, et al.. Aceclofenac and interactions analysis in the crystal and COX protein active site. *Journal of Molecular Structure*, 2020, 1205, pp.127600. 10.1016/j.molstruc.2019.127600 . hal-03011799

HAL Id: hal-03011799

<https://hal.science/hal-03011799>

Submitted on 18 Nov 2020

HAL is a multi-disciplinary open access archive for the deposit and dissemination of scientific research documents, whether they are published or not. The documents may come from teaching and research institutions in France or abroad, or from public or private research centers.

L'archive ouverte pluridisciplinaire **HAL**, est destinée au dépôt et à la diffusion de documents scientifiques de niveau recherche, publiés ou non, émanant des établissements d'enseignement et de recherche français ou étrangers, des laboratoires publics ou privés.

Aceclofenac and interactions analysis in the crystal and COX protein active site

Christian Jelsch^{a*}, Rajendran Niranjana Devi^{b,c}, Bruce C. Noll^d, Benoît Guillot^a, Israel Samuel^b, Emmanuel Aubert^a

^aCNRS UMR 7036 CRM2, Laboratoire de Cristallographie, Résonance Magnétique et Modélisations, Université de Lorraine, BP 70239, 54506 Vandoeuvre-lès-Nancy Cedex, France.

^b Research and post graduate department of Physics, The American College, Madurai – 625002, Tamil Nadu, India.

^c Department of Physics, Fatima college, Madurai -625 018, Tamil Nadu, India.

^d Bruker AXS Inc., Madison, Wisconsin, 53711, U.S.A

* christian.jelsch@univ-lorraine.fr.

Highlights

- The electron density of the Aceclofenac drug has been derived from ultra high-resolution X-ray diffraction at 0.35 Angstrom.
- Topological and electrostatic potential features of the crystal structure are presented
- Statistical analysis of intermolecular contacts within the crystal reveals the driving forces stabilizing the packing
- The interactions of Diclofenac in the complex with protein COX2 were analyzed.

Abstract

An experimental charge density analysis of the anti-inflammatory drug aceclofenac has been accomplished and compared with periodic Density Functional results. Diffraction data sets were measured on two crystals on a Bruker Photon II detector. The merging of the two data sets resulted in improved crystallographic *R*-factors. The analysis of the intermolecular contact types and their enrichments highlights the driving forces of the crystal packing. Strong hydrogen bonds C=O...H-O between carboxylic groups act as one of the main backbones in the crystal packing while halogen bonding Cl...O and the non-polar contacts C-H...Cl are also well represented. The C₆H₄Cl₂N heterocycle forms aromatic donor-acceptor parallel self-interactions through an inversion center while the less substituted C₆H₄N cycle is more involved in C-H... π interactions. The N atom linking the two phenyl rings presents mixed sp²/sp³ hybridization and bears a weak but visible electron lone pair.

The electrostatic potentials generated by the molecule and by its surrounding on the Hirshfeld surface were analyzed and show a good electrostatic complementarity for the charged regions of the molecule, while the non-polar regions interact with each other. The electrostatic energies computed between interacting dimers in the crystal show that the strongest dimer is the one forming two O-H...O hydrogen bonds. The electron density ellipticity and Laplacian values were analyzed on the covalent bonds critical points. The C-H bonds on the two aromatic C₆ rings have a modest but significant ellipticity value $\langle \epsilon \rangle = 0.048$, presumably due to the proximity of the C-C bonds with π character of the carbon atoms involved in the bonds. Theoretical geometry optimizations performed on the isolated molecule and on crystallographic dimers show the effect of the intermolecular interactions on the molecular conformation, which is slightly affected by the crystal packing.

The aceclofenac medicinal compound, metabolized into diclofenac after loss of an acetic acid group, binds *in vivo* to the target COX-2 protein. An electron density model of diclofenac has been derived from the refined electron density of aceclofenac. The interactions between diclofenac and the protein were analyzed from an electrostatic and Hirshfeld surface analysis points of views.

Keywords: electron density, Hirshfeld surface, contacts enrichment, electrostatics, drug-receptor interactions.

1. Introduction

Aceclofenac (ACF) acts as a first-line drug in the symptomatic treatment of rheumatoid arthritis, osteoarthritis and ankylosing spondylitis [1,2] The ACF molecule (Fig.1), 2-[2-[2-[(2,6dichlorophenyl)amino]phenyl]-acetyl] oxyacetic acid (C₁₆H₁₃Cl₂NO₄) [3-5] is the glycolic acid ester of diclofenac and is a cytokine inhibitor. ACF is actually transformed in vivo in Diclofenac (loss of an acetic acid group) and other metabolites [6,7]. ACF does not bind to cyclo-oxygenase (COX) proteins by itself. However, its metabolite Diclofenac blocks the action of the COX 1 and 2 which produce prostaglandin and causes pain, swelling and inflammation [8].

In general, non-steroidal anti-inflammatory drugs (NSAID) are the most widely used medications which mitigate pain and inflammation in many disorders. Some well-known carboxylic acid derivatives such as aspirin, ibuprofen, naproxen, diclofenac and mefenamic acid are powerful NSAID [9-13].

ACF bears a carboxylic acid; that chemical group is found in a wide range of pharmaceutical compounds and plays a cardinal role in drug design. Peculiarly, the carboxylic acids can act as both hydrogen bond acceptor and donor due to the simultaneous presence of carbonyl (C=O) and hydroxyl (O-H) groups. Hence carboxylic acids, which are quite polar in nature [14], can form dimers corresponding to homo-synthons well-known in supramolecular chemistry [15]. Aceclofenac is such a carboxylic acid derivative and one of the important non-steroidal anti-inflammatory drug (NSAID) molecules, which also possess analgesic properties. As ACF has poor solubility, the stability of ACF-lysine salt was investigated by [16] which showed a two orders of magnitude increase of the dissolution rate and of the solubility compared to ACF crystals.

An in-depth investigation of the charge density of a molecule from high-resolution X-ray diffraction at low temperature gives insights into the chemical bonding within molecules as well as into intra- and inter-molecular interactions in the crystal packing. Molecular similarity and recognition properties have a strong relationship with the structure and the electronic charge density [17]. Therefore, the accurate characterization of the molecular charge density through the topological analysis of electron densities and the study of the molecular electrostatic properties are essential for further useful processes like modeling and docking the drug into binding sites of target proteins. Indeed charge density is the source from which the one-electron properties along with the molecular topology, electrostatic potential, atomic and molecular moments could be easily

derived [18]. In addition, knowledge about electrostatic potential over the molecule provides a pathway to analyze drug-receptor interaction relationships.

In this study, structure factors of crystalline ACF were retrieved both from two low temperature X-ray diffraction experiments and a periodic *Density Functional Theory* calculation performed using *CRYSTAL14* [19] at the B3LYP/6-31G** level of theory. Topological analyses of the electron densities were carried out according to the quantum theory of atoms in molecules [20]. Some electron density derived properties such as Laplacian, atomic charges and electrostatic potential have been analyzed in order to throw light into the structural, electronic and molecular properties of the drug Aceclofenac.

In medicinal chemistry, it is well recognized that several factors play an important role in drug/target recognition processes. In the [21] review on molecular recognition, the primary roles of the steric and electronic distribution of a molecule, of water molecules in active sites and of desolvation effects are reported. Special attention was paid to the electrostatic interactions of Diclofenac (the active metabolite of aceclofenac) within protein COX-2 active site and an analysis of contacts at the Hirshfeld surface of the protein/ligand interface was carried out.

2. Materials and Methods

2.1. Crystallization

Crystals were grown by slowly evaporating an aqueous solution of ACF at room temperature (298K). High resolution X-ray diffraction experiments were performed on two selected good quality single crystals.

2.2. X-ray data collection and structure solution

Data were collected on Bruker D8 VENTURE/QUEST diffractometers using a MiTeGen mount in order to carry out the measurement at 100(1) K using a stream of cold nitrogen on an Oxford cryo-system [22]. Ultra-high resolution diffraction data sets were collected up to resolution 0.37 Å (see Table 1).

Determination of unit cell parameters through refinement, data collection and reduction were performed using program SAINT v8.38A software [23]. Program SADABS [24] was used for performing data sorting, scaling, absorption correction, and averaging. Two data sets were

measured on the two selected crystals. Each of the two data sets was merged on its own ($R_{\text{merge}} = 4.51$ and 3.12%). The two resulting I_{hkl} data sets were then merged, resulting in a R_{merge} factor of 4.06% .

The structure was solved with the *ShelXT* [25] structure solution program and refined with the *ShelXL-2017* [25] refinement package. Additional information on crystal data, measurement and refinement are given in Table 1.

[Table 1]

2.3. Charge density refinement

The experimental charge density refinement was carried out against all diffraction intensities using *MoPro* software [26] implementing the Hansen-Coppens multipole model for pseudo-atom electron density [27].

The chlorine atom was refined up to hexadecapoles, the atoms C, N, O were refined up to octapole level and the hydrogen atoms up to dipole level. The core and valence spherical scattering factors were calculated from [28] wave-functions and the anomalous dispersion coefficients were taken from the International Tables for Crystallography (2004).

The U_{ij} thermal displacements parameters were fixed for H atoms to the values computed by the *SHADE3* server [29], which was applied on the rigid fragments of the molecule.

The experimental and theoretical deformation maps were estimated and schemed with the help of *VMoPro* module of the *MoPro* software [26]. The 3D iso-surfaces representations and the molecular view with atomic displacement parameter ellipsoids were produced with *MoProViewer* [30]. An extinction coefficient [31] of the diffraction data was refined (isotropic, type 1, Gaussian, $E=0.10 \cdot 10^{-4}$ s). The crystallographic details of the experimental refinement are given in Table 1.

At first, the different parameter types were refined successively and finally all together till convergence. The H-X distances of H atoms were restrained to the standard values obtained from neutron diffraction studies [32] with a restraint sigma of 0.01 \AA . X-H distances similarity restraints were also applied to chemically equivalent groups (sigma= 0.01 \AA). Rigid bond and generalized rigid bond [33] restraints were applied to the anisotropic thermal ellipsoids of all non H atoms (sigma= 0.001 and 0.002 \AA^2 , respectively).

The expansion/contraction coefficients of H atoms were restrained to be similar ($\kappa \approx \kappa' \pm 0.01$). The κ coefficients of chlorine atoms were restrained to be similar to that of the theoretical charge density. The application of a local mirror symmetry constraints were deemed necessary for the O2 and O3 atoms to obtain a realistic charge density. Chemical equivalence similarity and local symmetry restraints were applied to the multipolar charge density of all other atoms, using a restrain sigma of 0.003.

As the residual Fourier map showed significant peaks around the two chlorine atoms and oxygen atoms O1 and O2, they were modelled with anharmonic thermal motion at order 3 [34]. A local mirror symmetry was applied on the charge density on these two oxygen atoms.

The *ssd* methodology [35] was used to estimate the uncertainty on topological properties (Laplacian and ellipticity) of the covalent bonds. This method is based on calculation of Sample Standard Deviations of properties using randomly perturbed charge density models, and is available within the *MoPro* software.

2.4. Theoretical calculations

Periodic quantum mechanical calculations were accomplished with program *CRYSTAL14* [19]. With the help of density functional theory (DFT) method and B3LYP hybrid functional completed with dispersion corrections [36], the optimization of hydrogen atom positions was performed keeping all other atoms and unit cell parameters fixed. The 6-31G** basis set, which was taken from EMSL Basis Set Library [37, 38] was used for all atoms.

The level of accuracy in evaluating the Coulomb and exchange series have been controlled by five parameters namely, $ITOL_i=8$, $i=1,4$ and $ITOL_5=18$. The shrinking factor of the reciprocal space was set to 6, corresponding to 80 k points in the irreducible Brillouin zone. After the convergence of the energy ($\Delta E \approx 10^{-8}$ Hartree) the periodic wave-function which is based on the optimized geometry was retrieved. The structure factors were calculated up to 0.5 Å resolution using the option XFAC of the *CRYSTAL14* [19] program. As U_{ij} thermal parameters were not refined and fixed to zero and as the deformation density contributes to diffraction mostly at atomic resolution, theoretical data were not extended to experimental resolution. A unitary weighting scheme was applied on the structure factors. For non-H atoms, a κ expansion/contraction coefficient applying to the core electrons was refined to diminish the high residual Fourier electron

densities occurring around atomic nuclei and which may partly arise from the use of Gaussian functions in theory vs. Slater functions in the *MoPro* refinement [39].

2.5 Geometry optimizations.

Optimization of isolated ACF molecule and of dimers were undertaken by Density Functional Theory calculations. The initial coordinates were taken from the X-ray experimental model and were optimized at the B3LYP-D3 6-311++G(d,p) level of theory using the Gaussian09 software [40].

2.6. Refinement of theoretical charge density

The theoretical multipolar refinement (hereafter called THEO) was executed versus the theoretical structure-factor amplitudes F_{hkl} . Multipolar parameters were refined up to the hexadecapole level for the Cl atom, up to octapole level for C, N and O atoms while one dipole D_z and one quadrupole Q_{zz} oriented along the X-H axis were refined for H atoms. The THEO refinement was performed up to 0.5Å resolution with unitary weighting scheme on F_{hkl} 's and the following options:

- (i) The atomic coordinates were kept fixed to the structure obtained after optimization of hydrogen atoms positions.
- (ii) The scale factor was fixed to unitary value.
- (iii) The atomic thermal motion parameters were set to zero.
- (iv) no constraints/restraints applied.

2.7. Diclofenac/COX2 model

ACF is related to the NSAID drug Diclofenac, from which it differs only by the presence of the oxy-acetic acid moiety at the O3 position (Fig. 1). This gives the opportunity to study the interaction between Diclofenac and active site residues of cyclo-oxygenase 2 (COX-2) from a charge density perspective. For this purpose, the 2.9Å resolution structure of murine COX-2 in complex with Diclofenac (PDB ID: 1PXX) has been retrieved from the Protein Data Bank [41]. Hydrogen atoms have been added to the protein using the *MolProbity* web server [42] using nuclear X-H distances options. Then an electron density model of diclofenac ligand was built based

on ACF theoretical refined parameters, excepted for its COOH group which was modelled using the appropriate electron density parameters as available in the ELMAM2 electron density database [43]. In a first model, the carboxylic group of diclofenac was in its protonated form as implied by the significantly different lengths of the C-O covalent bonds observed in the four monomers (average $d(\text{C1-O2}) = 1.224 \pm 0.003 \text{ \AA}$ vs $d(\text{C1-O1}) = 1.35 \pm 0.04 \text{ \AA}$). Eventually, the modelled diclofenac molecule was set electrically neutral by applying a small uniform shift of +0.00128e on the atomic valence populations. As a resolution of 2.9 Å is not enough to discriminate between a C=O and C-O-H group, the diclofenac molecule was also modelled with a carboxylate group (ELMAM2 derived), resulting in a global ligand charge of -0.57 e.

The electron density model of COX-2 protein atoms has been built using parameters transferred from the ELMAM2 library [43]. The atomic valence populations of residues whose centroid are located within 10Å of the ligand (including a single charged residue, Arg120) were shifted by +0.000395e so that the sum of their atomic charges reaches a formal charge of +1e.

3. Results and discussion

3.1. Structure description

The ACF structure has actually two aromatic rings capable of endorsing a twisted conformation relative to each other, as they are linked by a secondary amine N atom (Fig. 1). The molecule is a derivative of Diclofenac, whose free acid is prolonged by an acetic acid moiety, resulting in a longer side chain [44]. A previous room temperature study of ACF crystal structure was carried out by [45] in which they described a geometry of the molecule in close agreement with results reported in the present study. Nearly 1.7% of cell volume shrinkage is observed when the temperature was reduced from room temperature [45] to 100K (this study). For instance, among the five C-O bonds, C2-O3 is the longest: 1.42630(12) Å in this study; 1.442(4) Å in [45]. As noticed in the previously reported structure, the N lone pair is more delocalized towards the chlorinated ring than to the phenyl ring because the C11-N1 bond has smaller length (1.39784(11) Å) than C10-N1 (1.41575(11) Å). Similarly, as observed in the study by [45], the C-N-C angle (122.406(7)° here, 121.4(3)° in the previous study) lies close to 120°. On the other hand, the C11-N1-H1=113.28(16)° and C10-N1-H1=111.65(16) angles are close to 109°. Therefore, the N1 atom is in between a tetrahedral and a trigonal geometry which suggests a mixed sp^2/sp^3 hybridization.

The chiral volume of N atom with its three neighbors is 1.024 Å³ and the sum of angles is 347.4°, which is in between a tetrahedral (328°) and a trigonal (360°) geometry.

The deformation of C-C-C valence angles has been calculated for the two aromatic rings separately in order to measure the distortion in bond angles. The root means square deviations from the ideal 120° value of the hexagonal angles is computed as:

$$\sigma_{hex} = \sqrt{\sum_{i=1}^6 \frac{(\theta_i - 120^\circ)^2}{6}}$$

The distortion in angle found for the 2,6-dichlorophenyl ring is higher ($\sigma_{hex}=2.2^\circ$) than that of the phenyl ring 2 of the molecule ($\sigma_{hex}=0.8^\circ$), which can be attributed to the substituted Cl atoms and their electron withdrawing effect on the dichlorophenyl ring. The root mean square (rms) distance of the six carbon atoms from the mean C6 plane is 0.011 Å for both cycles. The CL1 chlorine atom is slightly out of the C6 aromatic plane at a distance of 0.120 Å, while the CL2 atom is closer to the plane at $d=0.011$ Å. This geometric distortion is most likely due to intramolecular steric clash with the aromatic ring, as in the molecule optimized *in vacuo*, the CL1 atom is still 0.09 Å out of the aromatic ring plane.

3.2. Crystal packing and contacts

In the crystal, four symmetry equivalent ACF molecules in the proximity of the asymmetric unit molecule engage in distinctly attractive interactions. The projection of the packing of ACF molecule along **b** axis (Fig. 2a) shows chains of molecules interacting in direction (2**a**+**c**).

Dichlorophenyl groups of ACF molecules, related by translation **b**, interact with each other and form a C-H⋯Cl hydrogen bond (Fig. 2b, Table2). There is also a CL1⋯CL2 contact between two such molecules forming a halogen⋯halogen bond in type II arrangement [46]; the interatomic distance ($d=3.4877(1)$ Å) is very close to the sum of their van der Waals radii (3.5 Å).

[Table 2]

The interactions between the acid ester chains are sustained by the O-H⋯O and C-H⋯O hydrogen bonding. The hydrogen bonds geometry parameters are given in Table 2. As found in all the other structures related to ACF [44, 47], there is an intramolecular hydrogen bonding of N-H⋯O type (Fig. 1): the N⋯O distance 3.02779(14) Å is close to the one found in the previous room

temperature study (3.019Å) [45]. Two dichlorophenyl C₆H₃Cl₂N heterocycles form also extensive aromatic donor–acceptor parallel stacking ($d=3.499\text{Å}$) through an inversion center (Fig. 2c), where electropositive and electronegative atoms interact with each other [48].

Generally, carboxylic acid COOH group likes to form a homodimer synthon with a group of another molecule because it possesses both an H-bond donor and acceptor [15]. In the ACF crystal structure, the COOH group interacts instead concomitantly with two COOH groups of two neighboring molecules to form two strong C=O⋯H-O hydrogen bonds (Fig. 2b). The carboxylic group is entirely dedicated to these intermolecular contacts creating molecular chains along the **b** axis. The ester carbonyl oxygen (O4) is on the other hand involved in dimer formation with a neighboring molecule through a double C2-H2B⋯O4 interaction (Fig. 2d).

The Hirshfeld surface analysis [50, 51] allows visualizing the intermolecular interactions. The fingerprint plots [52] use the inner and outer distances (d_i and d_e) to the Hirshfeld surface points. H⋯H contacts (Fig. 3a) play major role occupying 31.6% of the surface while the hydrogen bonds O⋯H (Fig. 3b) occupy the second largest area (20.7%) which gives two sharp and symmetric spikes at short distances, visible on the lower left corner of the fingerprint plot.

In order to analyze interaction propensities in molecular crystals, the contact enrichment applying to the different pairs of chemical species present in the structure was described in [53]. An enrichment ratio E_{XY} larger than unity for a particular contact between chemical species X⋯Y pinpoints that these are over-represented contacts in the crystal packing by comparison with equiprobable contacts. These latter proportions are derived by probability products, from the chemical composition on the Hirshfeld surface. The less polar H_c atoms bound to carbon were distinguished from the more electropositive H_{n/o} hydrogen atoms. Globally the lowly polar atoms (C, H_c, Cl) constitute as much as 82% of the molecular surface (Table 3).

[Table 3]

Evidently, the strongly electrostatic attractive O⋯H_{n/o} hydrogen-bonds ($E= 4.15$, Table 3) are recognized as the most favored contact among all other existing contacts. It concerns the intermolecular hydrogen bond C1=O1⋯H2-O2 between carboxylic groups but also longer distance weak interactions N1-H1⋯O2 and O2-H2⋯O3 ($d_{HO}>2.85\text{Å}$). Moreover, the intramolecular N-H⋯O=C strong H-bond is not counted in these intermolecular contact statistics. Although they represent only 5.4% of the Hirshfeld surface, the O⋯H_{n/o} contacts act as one of the main

backbones in the crystal packing. The weak hydrogen bonds between the lowly positively charged Hc atoms and oxygen atom occupy more than 12% of contact surface and are only very slightly enriched. Some close to zero enrichment ratios relate to O \cdots O and Hn/o \cdots Hn/o contacts and are absolutely evaded in the crystal system as they concern repulsive self-contacts between charged species.

Occupying the largest contact area in [Table 3](#) (19.3%), the non-polar Hc \cdots C contacts are neither enriched, nor disfavored at $E=0.99$ and consist notably of C-H $\cdots\pi$ interactions involving the least substituted C₆ aromatic cycle. The C \cdots C contacts represent 7.9% of the interaction surface and can be considered as a weakly favored contact as it has enrichment ratio $E=1.16$ and are related to the C₆H₄Cl₂N heterocycles forming parallel inverted stacking contacts ([Fig. 2c](#)). Heterocycles have a propensity to stack together as they can display some electrostatic complementarity [[48](#), [53](#), [54](#)]

Among non-polar contacts, the Cl \cdots Hc weak hydrogen bonds represent 16.5% of the Hirshfeld surface and are the most enriched at $E=1.26$. The non-polar Hc atoms are indeed good contact partners for organic halogen atoms [[55](#)] while contacts with the electropositive Hn/o atoms are generally avoided.

In summary, the crystal packing is maintained by highly over-represented strong hydrogen bonds (intra and inter-molecular N-H \cdots O and intermolecular O \cdots H-O) along with slightly enriched weak hydrogen bonds C-H \cdots O. Non-polar contacts between Cl, Hc and C species constitute however the majority of contacts (68%) and have all enrichment ratio not far from unity.

3.3 Analysis of optimized Dimers

Density functional theory calculations were undertaken on isolated ACF molecule and crystallographic dimers of molecules in order to probe the effect of the intermolecular interactions on the molecular conformation. The superposition of the experimental and isolated fully optimized molecules displayed in [Fig.4](#) shows that the main differences are associated with the positions of the acetoxy-acetic acid and dichloro-phenyl-amino chains relative to the central phenyl ring.

To get further insights on the origin of the differences affecting the dichloro-phenyl-amino chain orientation, dimers of two adjacent molecules related by translations along **b** direction were

analyzed. Dimers 1 and 2 are constituted by two molecules related by a translation of vector **b**. In dimer 1, the molecule directed towards [0,-1,0] direction was optimized (Fig.5a), while in dimer 2, the other molecule was optimized (Fig.5b). Only the atoms belonging to the acetoxy-acetic acid and dichloro-phenyl-amino chain of one of the molecules were optimized. All atoms of the other molecule and the atoms of the central phenyl ring of the first molecule were kept fixed at the experimental geometry.

The dichlorophenyl-amino group, after optimization within the dimer, moves slightly away and forms a lengthened CL2...CL1 contact with the neighboring molecule.

In the second dimer, dichloro-phenyl-amino group moves much less and makes the same CL1...CL2 contact but also a CL1...O4 halogen bond with the acetoxyacetic acid chain of the adjacent molecule (Fig. 5b).

Interestingly, the C5-C10-N1-C11 torsion angle implying the optimized molecule in the dimers reaches 168.39° for the first dimer, a value in between the experimental crystal (173.00°) and the isolated optimized molecule (163.00°) results. In the second dimer, the dihedral angle is 172.84°, a value very close to what is observed in the experimental X-ray structure. This shows that the ~10° change in the torsion angle (crystal vs. vacuo) is directly related to the intermolecular interactions, where the CL1...CL2 but also the CL1...O4 contacts seems significant.

The CL2...CL1 contact in dimer 1 appears attractive since the associated interatomic distance reduces from 3.99 Å (isolated molecule geometry) to 3.69 Å in the optimized dimer 1 (Fig. 5a). In the dimer 2, the same contact appears also as attractive (CL1...CL2 distance reducing from 3.69 Å to 3.53 Å (Fig. 5b). This can be rationalized by noticing that C16-CL2...CL1 forms a typical type-II halogen bond, albeit long in the crystal structure (CL2...CL1=3.488 Å; C16-CL2...CL1=162.50°; C-CL1...CL2=104.40°). The positively charged sigma hole of CL2 faces the negative crown of CL1.

On the other hand, the CL1 atom forms a halogen bond with the O4 carbonyl atom, the distance $d=3.090$ Å being shorter than the van der Waals contact ($d=3.27$ Å) and the C12-CL1...O4 angle is 165.90° which is not far from 180°. Both CL1 and O4 have negative charges (Table 4) but the electrostatic interaction can be attractive for C-Cl...O $\approx 180\pm 20^\circ$ geometries when the halogen sigma hole faces the electronegative oxygen atom [56]. The CL1...O4 contacts seems however

repulsive with *in vacuo* optimized conformation as it is associated to a very short distance $d=2.75\text{\AA}$; in the optimized dimer conformation, it is increased to 3.05\AA (Fig. 5b).

[Table 4]

Similarly, the CL2 \cdots H13 contact distance increases, in dimer 2, from 2.32\AA in the *in vacuo* conformation to 2.90\AA in the dimer optimized structure (Fig. 5b). The CL2 \cdots H13 electrostatic favorable interaction has to comply with the van der Waals distances ($1.75+1.20=2.95\text{\AA}$) since the aromatic H13 atom is not acidic enough to make such a shortened hydrogen bond with the chlorine atom.

The electron density value at the critical point characterizing the CL1 \cdots CL2 contact reaches ($0.0451(1)\text{ e/\AA}^3$) and the positive Laplacian value ($0.548(4)\text{ e/\AA}^5$) relates to the closed shell character of the interaction (Table 2). These values are in accordance with those found in C_6Cl_6 and $\text{C}_6\text{Cl}_5\text{OH}$ crystal structures [57] where ρ_{cp} is in the $0.038 - 0.058\text{ e/\AA}^3$ range and $\nabla^2\rho_{\text{cp}}$ in the $0.41 - 0.62\text{ e/\AA}^5$ range. It appears, on the basis of the electron density value at the bond critical point ($\rho_{\text{cp}}=0.0228\text{ e/\AA}^3$ in Table S1), that the CL2 \cdots H13 hydrogen bond is weaker than the halogen \cdots halogen interaction.

3.4 Deformation electron density

Static deformation electron density $\Delta\rho$ maps of the dichlorophenyl ring and of the ester group are shown in Fig. 6a,b and Fig. 6c, respectively. The dichlorophenyl ring plane is parallel to the **b** direction, therefore two such rings related by **b** translation are in the same plane. Generally, a σ or π hole can be seen as positive electrostatic potential on unpopulated σ^* or $\pi^{(*)}$ orbitals and they are able to interact with some electron rich groups. A σ -hole is typically located along the vector of a covalent bond such as X-H or X-Y (X=any atom, Y=halogen). The H and Y atoms are respectively known as hydrogen and halogen bond donors. Fig. 6a shows the clear visualization of the presence of sigma hole of CL1 and CL2 atoms, resulting in polar flattening effect. The relative orientation of the CL1 \cdots CL2 atoms permits the positive sigma hole of CL2 to face the negative crown of CL1. The CL1 \cdots O4 halogen bond and the CL2 \cdots H13 hydrogen bond are also visible in Fig. 6a.

The N1 nitrogen atom, bound to the two phenyl rings, has partial sp^2/sp^3 character, as it has a weak electron lone pair which is visible in the experimental (Fig. 6d) and in the theoretical $\Delta\rho$ maps.

The experimental and theoretical $\Delta\rho$ maps display globally a correlation coefficient of 78% and very similar rms values over the asymmetric unit: $\text{rms}(\Delta\rho_{\text{theo}})=0.084$ and $\text{rms}(\Delta\rho_{\text{exp}})=0.089\text{ e}/\text{\AA}^3$.

3.5. Topological analysis of the molecular charge density

The topological properties of covalent bonds (Ellipticity and Laplacian values) are shown in Fig. 7 and 8. For the aromatic ring C-C bonds, the nature of the bound neighbors, which can be chlorine or nitrogen atoms, is also accounted for. Fig. 8 shows that, most of the time, the chemical clustering is reflected in the Laplacian values. For instance, all C-H bonds present Laplacian values comprised between $-14.1(2)$ and $-16.9(3)\text{ e}/\text{\AA}^5$. Ring C-C bonds are also clustered with higher Laplacian values ranging between $-17.1(2)$ and $-19.1(1)\text{ e}/\text{\AA}^5$. This group is noteworthy as Laplacian values are found similar within one *ssd* for C-C bonds sharing identical neighbor atoms, as it can be seen in Fig. 8 for pairs of C-C(-Cl), C-C(-N) and (N-)C-C(-Cl) bonds. The *ssd* of the Laplacian on the six (C-)C-C(-C) bonds represents only 2.1% of the $-18.2\text{ e}/\text{\AA}^5$ average value.

Excepted in the aromatic cycles, the C-H bonds present generally relatively low ε ellipticities, characteristic of cylindrical single bonds, and are all comparable within three *ssd* values. The ε values of C-H bonds in the aromatic cycles have an average value of 0.048 and standard deviation of 0.018 while the average uncertainty (estimated by *ssd* methodology) is 0.005. These bonds have a small but significantly different from zero ellipticity, as shown by the deformation maps in the plane perpendicular to the C14-H14 bond (Fig. 6b), due to their partial π character. The C-H bonding density is slightly elongated in the direction perpendicular to the aromatic plane, in a less pronounced way to what is observed in aromatic C-C bonds, and is presumably due to the sp^2 character of the carrier carbon atom.

The C-C bonds in the aromatic rings display ellipticity values ranging between 0.203(9) and 0.291(4), corresponding to bonds with π character. The average ε value is 0.238 and the standard deviation within the sample is 0.029, which is more than five times the average uncertainty of 0.005 obtained by *ssd* method. This implies that some discrepancies of ε are statistically significant. Comparing the C-C bond ellipticities within the two aromatic C6 rings, shows that the dichloro-substituted ring presents more disparate values. The C14-C15 and C14-C13 bonds (located at the extremity of the ring) have a significantly more single bond character

than the C11-C16 and C11-C12 bonds which are connected to the amino group. This effect is related to the delocalization of the N1 electron lone pair in favor of the chlorinated ring, as already seen by the shorter N1-C11 bond compared to N1-C10.

The N1 lone electron pair (LP) has been further characterized by the mean of a topological analysis of the $L(\mathbf{r})$ function (minus Laplacian of the electron density) in the region of the amino group. This allowed evidencing a (3,-3) critical point, *i.e.* a local maximum of $L(\mathbf{r}) = 51 \text{ e}/\text{\AA}^5$, corresponding to a point of valence shell charge concentration (VSCC) associated to the N1 nitrogen lone pair. In addition to the aforementioned geometrical considerations describing the N1-H1-C10-C11 group, analysis of the position of this critical point with respect to N1 again supports its partial sp^2/sp^3 character. Indeed, the VSCC point evidenced in $L(\mathbf{r})$ is located 0.40 Å away from N1 atom, that is, at a distance significantly shorter than the one measured, on the basis of DFT-computed electron localization function (homeomorphic to the Laplacian), in ammonia where the N-LP distance reaches 0.65Å [58]. Moreover, LP-N1-C11, LP-N1-C10 and LP-N1-H1 angles in ACF are 104°, 93° and 109° respectively, indicating a distorted, slightly flatter geometry than the one expected for a pure sp^3 nitrogen.

Electron delocalization effects can also be described in the oxy-acetic acid moiety. Indeed, the formally single bonds formed by the O3 ester atom have significant ellipticity: C3-O3 ($\varepsilon=0.074(9)$) and C2-O3 ($\varepsilon=0.075(9)$) as well as the C1-O2 single bond in the carboxylic acid ($\varepsilon=0.046(7)$). Such values illustrate their partial π character due to resonance with the C3=O4 carbonyl group which, consequently, displays a low ellipticity value ($\varepsilon=0.078(7)$) for a formally double bond. The O1=C1 bond however, which is also formally double, presents a high ellipticity reaching 0.150(9).

3.6. Atomic charges

Electron density integration over atomic basins provides atomic charges which reveal the electrostatic nature of atoms. The Bader atomic charges derived from both theoretical and experimental charge densities are given in Table 4. Integrated charges obtained from the two models agree well, with a correlation coefficient reaching 98%. The only notable discrepancy can be seen for the charge of the hydroxyl H2 polar hydrogen atom, which appears significantly more positively charged in the experimental electron density than in the THEO model. Nevertheless,

both models describe a very polarized O2-H2 bond. The two CH₂ groups are electron donating and they exhibit indeed positive charges. All oxygen atoms exhibit very strong negative charges ($Q \approx -1e$) and the C1 carbon atom in the carboxylic group shows the most positive charge ($Q \approx +1.54e$, Table 4) and is therefore the most prone to undergo nucleophilic attack. The ester carbonyl carbon atom C3 exhibits the next largest positive charge ($Q \approx +1.42e$) as it is attached to another very negative oxygen, the carbonyl O4 atom. Hence the most electronegative regions of ACF molecule are seen in the vicinity of the two carbonyl O=C oxygen atoms which are slightly more electronegative when compared to the O2 (C-O-H) and O3 (C-O-C) oxygen atoms. The N1-H1 and O2-H2 bonds are very polarized as the N1 and O2 atoms have strong negative charges (Q close to $-1e$) while H1 and H2 atoms have positive charges (0.42 and 0.62e, respectively). On the whole, the charge distribution in the ACF molecule can be characterized as a mixture of electrophilic/nucleophilic zones and of less polar aromatic rings.

3.7. Electrostatic potential and interaction energy

The electrostatic potential $V(\mathbf{r})$ mapped on the Hirshfeld inter-molecular surface provides pathway to assess the electrostatic complementarity around the molecule [59]. Fig. 9 shows the electrostatic potential $V_{\text{int}}(\mathbf{r})$ and $V_{\text{ext}}(\mathbf{r})$ on the Hirshfeld surface generated by the ACF molecule and by its contacting neighbors, respectively. The electronegative $V_{\text{int}}(\mathbf{r})$ region is found in the vicinity of oxygen atoms, as expected from the atomic charges distribution, whereas the positive $V_{\text{int}}(\mathbf{r})$ region is seen in the vicinity of the hydrogen atoms. As expected in terms of electrostatic potential complementarity, this is reversed for the potential $V_{\text{ext}}(\mathbf{r})$ generated by the cluster of adjacent molecules (Fig. 9b).

Fig. 10 illustrates a scatter-plot of electrostatic potential $V_{\text{int}}(\mathbf{r})$ and $V_{\text{ext}}(\mathbf{r})$ values on points sampling the Hirshfeld surface. The figure is nearly symmetric with respect to the diagonal line $V_{\text{int}} = V_{\text{ext}}$. The regions of strongest positive potential correspond to the H-O and H-N hydrogen atoms which interact with the electronegative regions around the oxygen atoms, resulting in H \cdots O hydrogen bonds. The Cl \cdots H/H \cdots Cl interactions are also highlighted in Fig. 10. Globally, the potentials $V_{\text{ext}}(\mathbf{r})$ and $V_{\text{int}}(\mathbf{r})$ are more electronegative on the chlorine atoms surface than on hydrogen atoms. The electrostatic potential is generally much smaller in magnitude on the Hirshfeld surface for the Cl \cdots H interactions than on the more polar O \cdots H ones. Globally the exterior and interior $V(\mathbf{r})$ values show a good complementarity as the correlation coefficient reaches -58%.

[Table 5]

The electrostatic energy of the different interacting dimers is shown in Table 5. The dimer with the strongest E_{elec} interaction energy (-66.8 kJ/mol) involves the bifurcated H-bonds O1 \cdots H2-O2, O3 \cdots H2-O2 and the weaker C4-H4B \cdots O1 hydrogen bonds (symmetry $^{3/2-x, -1/2+y, 3/2-z}$).

The second strongest dimer at -28.5 kJ/mol is formed around an inversion center (-x, 1-y, 1-z) with stacking of two dichloro-phenyl groups. The third dimer at -25.2 kJ/mol is related by an inversion center (1-x, 2-y, 1-z); it has a large interaction surface and includes twice the C2-H2B \cdots O4 weak hydrogen bond. The fourth dimer at -19.2 kJ/mol forms notably the CL1...C3 stacking contact and long distance C4-H4A \cdots N1 weak hydrogen bond ($d_{HN}=2.787$ Å) around the (1-x, 1-y, 1-z) inversion center .

3.8. Electrostatic interactions of diclofenac with protein COX-2.

It is known that the non-steroidal anti-inflammatory drugs Aceclofenac does not affect COX isoforms but instead is transformed to active metabolites (such as diclofenac) which, in turn, binds to COX-2 [6]. The chemical proximity of Diclofenac (DCF) and ACF allows to extract the charge density information from ACF and to transfer it to the structure of DCF, as bound to murine COX-2 structure (PDB ID:1PXX; [8]). In several other structures of COX2 complexes, for instance with ibuprofen or aspirin, the carboxylate group forms an ionic bridge with an arginine 120 residue [8]. The structure of the protein complexed with DCF revealed that the ligand binds to COX-2 in an “inverted conformation” where the carboxylic acid is hydrogen bonded to Tyr385 and Ser530 (Fig. 11). Moreover, site-directed mutagenesis data highlighted the predominant role of Ser530, whose mutation into alanine almost abolishes inhibition of COX-2 by Diclofenac. Conversely, diclofenac inhibition was unaffected by the mutation of Arg-120 to alanine.

Transferred multipolar electron densities distributions of DCF and COX-2 allow computing electrostatic interaction energies E_{elec} between the ligand and 18 residues lining the binding pocket. As the diclofenac/COX-2 structure presents two dimers per asymmetric unit, computations were performed on each of the four monomers, so that E_{elec} values presented in Table 6 are averaged with their estimated errors (standard deviations on the sample of four monomers). Due to the low resolution 2.8Å of the protein crystal structure, it is not clear if the DCF ligand is in its carboxylate or carboxylic acid form, hence the two possibilities have been considered

Fig. 11a shows the conformation of the bound DCF which is partly determined by a strong intramolecular hydrogen bond between the N-H group and an oxygen of the (COOH/CCO⁻) group. There is also an intramolecular contact at ~3Å distance between a chlorine atom and the (OH/O⁻) moiety. The Cl^{δ-}... (O^{δ-}-H^{δ+}) interaction appears more attractive than Cl^{δ-}...O^{δ-} from an electrostatic point of view, which indicates that, from this point of view, the diclofenac molecule is more likely to have a protonated COOH group.

Results on the non-charged, protonated DCF allow defining four categories of residues depending on their relative contribution to the diclofenac/COX-2 total electrostatic interaction energy, reaching $E_{elec} = -186(23)$ kJ.mol⁻¹.

[Table 6]

At first, there are two residues with large stabilizing contributions, Ser530 and Tyr385, whose electrostatic interaction energies with DCF have a magnitude larger than -50 kJ.mol⁻¹. These two residues contribute together to two thirds of the total stabilizing interaction energy between DCF and COX-2 binding site. The large contribution of Ser530 is coherent with the presence of two strong O-H...O hydrogen bonds between the side chain hydroxyl group and the carboxylic acid of DCF. This highlights the importance of Ser530 in the prostaglandin synthase inhibitor binding. The mutant S530A has an IC₅₀ value for DCF increased to >50nM compared to 77 nM for the wild type [8]. The Tyr385 phenol oxygen atom forms an O...H-C weak hydrogen bond with a CH₂ group of diclofenac.

Then, there is a set of three residues (Val349, Trp387 and Leu352) which present stabilizing energies stronger than -10 kJ/mol. The Val349 and Leu352 residues are located within the close vicinity of the DCF carboxylic group. The electronegative regions around the COOH moieties lead to a stabilizing contribution when interacting with the slightly positively charged CH₂ and CH₃ hydrogen atoms of Val349 and Leu352 side chains pointing inward the binding pocket. The side chain of Trp387 is interacting with the C₆NCH₄ aromatic ring bearing the CH₂-COOH group.

There is a series of eight non-polar amino acids, comprising aliphatic (Val349, Val523, Leu384, Met522) and aromatic (Phe381, Phe205, Phe518) residues, whose electrostatic interaction energies with diclofenac are weakly stabilizing, comprised between -2 and -11 kJ/mol. Beyond favorable non-polar contribution to the binding energy, one can associate to these residues, it appears that they also favor diclofenac binding from an electrostatic point of view. In this group, Met522 represents a special case as its favorable electrostatic interaction energy with diclofenac of $E_{elec} = -5.5(8)$ kJ/mol is attributable to a weak O \cdots H-C hydrogen bond formed between its carbonyl main chain oxygen and a hydrogen atom of the C₆NCH₄ ring of the ligand.

Three residues (Ser353, Ala527 and Tyr355) present very weak electrostatic interaction energies with DCF which are smaller than their associated *ssd*'s.

When the charged, carboxylate form of DCF is considered, the energy results show some significant differences (Table 6). Tyr385 and Ser530 still show strong energy values as their hydroxyl group is hydrogen bond donor to the carboxylate moiety. Residues Val 349, Leu 531, Trp 387, Leu 384, Leu 352, Val 523, Phe 205 and Phe 381 show all enhanced attractive electrostatic energies, which is due to the favorable interaction between the global negative charge of DCF and the numerous H δ^+ -C groups on these lowly polar residues. The favorable binding of partially hydrated anions to hydrophobic environments has been reported [60]. Globally, the summation of the E_{elec} energies over the active site residues yields a value which is 64% higher compared to the non-charged DCF molecule.

3.9. Hirshfeld surface analysis of diclofenac/COX-2 complex.

The DCF ligand is buried in a cavity of the COX-2 protein. Fig. 11b shows the interaction between the diclofenac drug and the COX protein active site. The protein surface in contact with diclofenac is mostly non-polar, as the Hc and C species constitute 77% of the interface area. This is also the case for the ligand as Hc and C species amount to 63% of the DCF surface with the additional presence of non-polar organic chlorine at more than 20%.

The three major contact types are of non-polar nature C \cdots Hc/Hc \cdots C, followed by Hc \cdots Hc and Cl \cdots Hc (Table 7) which account to 28, 19 and 18% of the surface, respectively. The chlorine

atoms interact mostly with weakly positively charged Hc hydrogen atoms and this contact type is enriched at $E=1.3$ while the contacts with all other atoms are disfavored.

[Table 7]

The O \cdots Ho/n and reciprocal Ho/n \cdots O contacts have the highest enrichment value although they account only for 5.3% of the contact surface. They constitute a driving force in the ligand binding and the carboxylic acid forms. There are two hydrogen bonds with the Ser530 hydroxyl group, once as acceptor and once as donor. The DCF COOH group is also accepting a H-bond from Tyr385. The Hn atom of diclofenac is still involved in an intramolecular hydrogen bond but with the C-O-H and not the C=O oxygen atom.

All the non-polar contacts involving C and Hc are slightly enriched except Hc \cdots Hc which is slightly under-represented as Hc is involved in C-H \cdots π interactions (H \cdots C) and weak hydrogen bonds with O and Cl atoms. Self-contacts are avoided, except for C \cdots C. The DCF C₆NCH₄ aromatic cycle is in contact with the peptidic trigonal carbon atom of Gly526 on one side and forms a stacking with Phe518 at long distance on the other side. Globally, the differences in the four independent protein/ligand structures are not significant and result in only small differences in the contacts statistics.

4. Conclusion

An extensive analysis was done on experimental crystal structure of the drug Aceclofenac complemented by a charge density study. The distortion in valence C-C-C angles from the perfect hexagon is larger for the dichloro substituted ring than for the other phenyl ring due to the substituted Cl atoms and their electronic effect. The accurate mapping of the charge distribution in molecules enables a better understanding of their interactions. Similarly to related structures, the ACF molecule also has intramolecular hydrogen bonding N-H \cdots O. The COOH group of ACF does not form the homo-synthon described by Desiraju [15]. Instead the carboxylic acid interacts with two COOH groups of two neighboring molecules to form two strong C1=O1 \cdots H2-O2 hydrogen bonds. Obviously, the strongly electrostatic attractive O \cdots H-N and O \cdots H-O hydrogen bonds have been recognized as the most statistically over-represented among all contacts in the ACF crystal. Non-polar C \cdots C contacts and weakly electrostatic C-H \cdots Cl interactions are also

avored. Halogen···Halogen Cl···Cl and halogen bonding Cl···O occur in the same region of the crystal but are slightly under-represented.

In vivo, the ACF molecule is metabolized into diclofenac. The interactions of protein COX-2 with resulting ligand diclofenac were analyzed and point out the most important contributing residues. The polar residues Tyr385 and Ser530 forming hydrogen bonds show the strongest electrostatic interaction energy while several non-polar residues interacting with the dichloro substituted phenyl ring of diclofenac have also significant electrostatic contribution.

Acknowledgements

The authors are grateful to the principal and secretary and the head of PG physics department of The American College, Madurai, India for their continued encouragement and support during the progress of this work. The CINES/CEA CCRT/IDRIS is thanked for allocation of computing time (project A0030807449). The EXPLOR mesocentre is thanked for providing access to computing facility (project 2017CPMXX0084).

Compliance with ethical standards

Conflict of interest: The authors declare that they have no conflict of interest.

Ethical statement: All ethical guidelines have been adhered.

References

- [1] B. Appa Rao, M.R, Shivalingam, Y.V. Kishore Reddy, Somesekhara Rao, K. Rajesh, & N. Sunitha, Formulation and evaluation of aceclofenac solid dispersions for dissolution rate enhancement, *Int. J. Pharm. Sci. Drug Res.*2 (2010) 146-150.
- [2] K.T. Shahanas, K.V. Shahida, K. Shareefa, M. Shereehan, G.R. Prasobh & S. Shrikumar, A review on evaluation of aceclofenac niosomes prepared by various techniques, *World J. Pharmacy and Pharmaceutical Sciences*, 5 (2015) 403-413.
- [3] K. Saurabh & K. Dharamveer, Development and Validation of analytical methods for Simultaneous Estimation of Diacerein and Aceclofenac in Bulk and Tablets using UV-visible spectroscopy, *Int. J. Chem. Tech. Res.* 2 (2010) 1816-1822.
- [4] R. Sangram Kumar, S. Rashmi Ranjan, P. Susanta Kumar, D. Arun Kumar, R. Satyanarayana, N. Srikant, UV- spectrophotometric method for simultaneous estimation of drotaverine hydrochloride and aceclofenac in bulk and their formulation, *Int. J. of Biol. & Pharma. Research*, 2 (2011) 55-59.

- [5] P. Trivedi, A.M.L. Verma & N. Garud, Preparation and characterization of aceclofenac microspheres, *Asian J. Pharmaceutics*.2 (2008) 110-115.
- [6] B. Hinz, T. Rau, D. Auge, U. Werner, R. Ramer, S. Rietbrock & K. Brune, Aceclofenac spares cyclooxygenase 1 as a result of limited but sustained biotransformation to diclofenac, *Clinical Pharmacology&Therapeutics*, 74 (2003) 222-235.
- [7] R. Niranjana, A.D. Stephen, P. Justin, K. Saravanan, P. Macchi, & C. Jelsch, Topological and electrostatic properties of diclofenac molecule as a non-steroidal anti-inflammatory drug: An experimental and theoretical study, *J. Mol. Struct.* 1196 (2019) 42-53,
- [8] S.W. Rowlinson, J.R. Kiefer, J.J. Prusakiewicz, J.L. Pawlitz, K.R. Kozak, A.S. Kalgutkar, W.C. Stallings, R.G. Kurumbail & L.J. Marnett. A novel mechanism of cyclooxygenase-2 inhibition involving interactions with Ser-530 and Tyr-385, *J. Biol. Chem.*, 278 (2003) 45763-45769.
- [9] A.D. Stephen, V.R. Hathwar, T.N. Guru Row & P. Kumaradhas, Topological Electron Density Analysis and Electrostatic Properties of Aspirin: An Experimental and Theoretical Study, *Cryst. Growth Des.* 12 (2012) 4357–4366.
- [10] N. Bouhaida, M. Dutheil, N.D. Ghermani, & P. Becker, Gradient vector field and properties of the experimental electrostatic potential: Application to ibuprofen drug molecule, *J. Chem. Phys.*, 116 (2002) 6196-6204.
- [11] M. Bešter-Rogač, Nonsteroidal Anti-Inflammatory Drugs Ion Mobility: A Conductometric Study of Salicylate, Naproxen, Diclofenac and Ibuprofen Dilute Aqueous Solutions, *Acta Chimica Slovenica*. 56 (2009) 70-77.
- [12] M. T. Donnelly, C.J. Hawkey, Review article: COX–II inhibitors—a new generation of safer NSAIDs?, *Aliment. Pharmacol. Ther.* 11, 1997, 227.
- [13] N. Okulik & A.H. Jubert, Theoretical Analysis of the Reactive Sites of Non–steroidal Anti–inflammatory Drugs, *Internet Electron.J.Mol.Des.*,4 (2005) 17–30.
- [14] R.W. Gora, S.J. Grabowski & J. Leszczynski, Dimers of formic acid, acetic acid, formamide and pyrrole-2-carboxylic acid: an ab initio study, *J.Phys.Chem.*109 (2005) 6397-6405.
- [15] G.R. Desiraju, Supramolecular Synthons in Crystal Engineering—A New Organic Synthesis, *Angew. Chem. Int. Ed.*34 (1995) 2311–2327.
- [16] N.R. Goud, K. Suresh & A. Nangia, Solubility and stability advantage of aceclofenac salts. *Crystal Growth & Design*, 13 (2013) 1590-1601.
- [17] R. Flaig, T. Koritsánszky, R. Soyka, L. Häming, & P. Luger, Electronic Insight into an Antithrombotic Agent by High-Resolution X-Ray Crystallography This work was funded by the Bundesministerium für Bildung, Wissenschaft, Forschung und Technologie (BMBF), Bonn (Germany) (grant no. 05 SM8KEA0) and by the Fonds der Chemischen Industrie, Frankfurt (Germany), *Angewandte Chemie Int. Ed.*40 (2001) 355-359.

- [18] P. Munshi & T.N. Guru Row, Charge density based classification of intermolecular interactions in molecular crystals, *Cryst. Eng. Comm.*, 7 (2005) 608-611.
- [19] R. Dovesi, R. Orlando, A. Erba, C.M. Zicovich-Wilso, B. Civalleri, S. Casassa, L. Maschio, M. Ferrabone, D.L. Perre, P.D. Arco, Y. Noel, M. Causa, M. Rerat & B. Kirtman, CRYSTAL14: A program for the *ab initio* investigation of crystalline solids, *Int. J. Quantum Chem.* 114 (2014), 1287-1317.
- [20] R.F.W. Bader, *Atoms in Molecules. A Quantum Theory*; Oxford University Press: Oxford, UK. (1990).
- [21] E. Persch, O. Dumele & F. Diederich, Molecular recognition in chemical and biological systems, *Angew. Chem. Int. Ed.*, 54 (2015) 3290 – 3327.
- [22] J. Cosier, & A.M. Glazer, A nitrogen-gas-stream cryostat for general X-ray diffraction studies, *J. Appl. Cryst.* 19 (1986) 105–107.
- [23] Bruker (2016) SAINT, v. 8.38A. Bruker AXS Inc., Madison, WI, USA.
- [24] L. Krause, R. Herbst-Irmer, G.M. Sheldrick & D. Stalke, Beyond the International Year of Crystallography, *J. Appl. Cryst.* 48 (2015) 3–10.
- [25] G.M. Sheldrick, Crystal structure refinement with *SHELXL*, *Acta Crystallogr. C* 71, (2015) 3-8.
- [26] C. Jelsch, B. Guillot, A. Lagoutte, C. Lecomte, Advances in protein and small molecule charge-density refinement methods using MoPro, *J. Appl. Crystallogr.* 38 (2005) 38-54.
- [27] N.K. Hansen, P. Coppens, Testing aspherical atom refinements on small molecule data sets, *Acta Crystallogr. A* 34 (1978) 909-921.
- [28] Z. Su, P. Coppens, Relativistic X-ray elastic scattering factors for neutral Atoms $Z=1-54$ from multi configuration Dirac-Fock wavefunctions in the $0-12\text{\AA}^{-1}\sin\theta/\lambda$ range, and six-Gaussian analytical expressions in the $0-6\text{\AA}^{-1}$ Range, *Acta Crystallogr. A* 53 (1997) 749-762.
- [29] A.Ø. Madsen, A.A. Hoser, SHADE3 server: a streamlined approach to estimate H-atom anisotropic displacement parameters using periodic *ab initio* calculations or experimental information, *J. Appl. Crystallogr.* 47 (2014) 2100e2104.
- [30] B. Guillot, E., Enrique, L., Huder, & C. Jelsch. (2014). MS19. O01. MoProViewer: a tool to study proteins from a charge density science perspective. *Foundations of Crystallog.* 70, C279.
- [31] P.J. Becker, & P. Coppens, Extinction within the limit of validity of the Darwin transfer equations. I. General formalism for primary and secondary extinction and their applications to spherical crystals *Acta Crystallogr. A*, 30 (1974) 129-147,
- [32] F.H. Allen & I.J. Bruno, Bond lengths in organic and metal-organic compounds revisited: X-H bond lengths from neutron diffraction data, *Acta Crystallogr. B* 66 (2010) 380–386.
- [33] A. Thorn, B. Dittrich & G.M. Sheldrick, Enhanced rigid-bond restraints, *Acta Crystallogr. A* 68 (2012) 448-451.
- [34] W.F. Kuhs, The Anharmonic temperature factor in crystallographic structure analysis, *Aust. J. Phys.*, 41 (1988) 369-82.

- [35] B. Fournier, B. Guillot, C. Lecomte, E.C. Escudero-Adán & C. Jelsch, A method to estimate statistical errors of properties derived from charge-density modelling, *Acta Crystallogr. A* 74 (2018) 170-183.
- [36] S. Grimme, Semiempirical GGA-type density functional constructed with a long-range dispersion correction. *J. Comput. Chem.* 27 (2006) 1787-1799.
- [37] K.L. Schuchardt, B.T. Didier, T. Elsethagen, L. Sun, V. Gurumoorthi, J. Chase, J. Li & T.L.J. Windus, Basis set exchange: a community database for computational sciences, *Chem. Inf. Model.* 47 (2007) 1045-1052.
- [38] D. Feller, The role of databases in support of computational chemistry calculations *J. Comp. Chem.*, 17(13) (1996) 1571-1586.
- [39] M. Ahmed, A. Nassour, S. Noureen, C. Lecomte, & C. Jelsch, Experimental and theoretical charge-density analysis of 1,4-bis(5-hexyl-2-thienyl)butane-1,4-dione: applications of a virtual-atom model *Acta Crystallogr. B* 72 (2016) 75-86.
- [40] M.J. Frisch, G.W. Trucks, H.B. Schlegel, G.E. Scuseria, M.A. Robb, J.R. Cheeseman, G. Scalmani, V. Barone, B. Mennucci, G.A. Petersson, H. Nakatsuji, M. Caricato, X. Li, H.P. Hratchian, A.F. Izmaylov, J. Bloino, G. Zheng, J.L. Sonnenberg, M. Hada, M. Ehara, K. Toyota, R. Fukuda, J. Hasegawa, M. Ishida, T. Nakajima, Y. Honda, O. Kitao, H. Nakai, T. Vreven, J.A. Montgomery Jr., J.E. Peralta, F. Ogliaro, M. Bearpark, J.J. Heyd, E. Brothers, K.N. Kudin, V.N. Staroverov, R. Kobayashi, J. Normand, K. Raghavachari, A. Rendell, J.C. Burant, S.S. Iyengar, J. Tomasi, M. Cossi, N. Rega, J.M. Millam, M. Klene, J.E. Knox, J.B. Cross, V. Bakken, C. Adamo, J. Jaramillo, R. Gomperts, R.E. Stratmann, O. Yazyev, A.J. Austin, R. Cammi, C. Pomelli, J.W. Ochterski, R.L. Martin, K. Morokuma, V.G. Zakrzewski, G.A. Voth, P. Salvador, J.J. Dannenberg, S. Dapprich, A.D. Daniels, Farkas, J.B. Foresman, J. V Ortiz, J. Cioslowski, D.J. Fox, Gaussian09 Revision D.01, Gaussian Inc, Wallingford CT, 2010.
- [41] H.M. Berman, J. Westbrook, Z. Feng, G. Gilliland, T.N. Bhat, H. Weissig, I.N. Shindyalov, & P.E. Bourne, The Protein Data Bank, *Nucleic Acids Research*, 28 (2000) 235-242.
- [42] V.B. Chen, W.B.III. Arendall, J.J. Headd, D.A. Keedy, R.M. Immormino, G.J. Kapral, L.W. Murray, J.S. Richardson, & D.C. Richardson, MolProbity: all-atom structure validation for macromolecular crystallography, *Acta Crystallogr. D* 66 (2010) 12-21.
- [43] Domagała, S., Fournier, B., Liebschner, D., Guillot, B., & Jelsch, C. (2012). An improved experimental databank of transferable multipolar atom models—ELMAM2. Construction details and applications. *Acta Crystallogr. A*, 68 (2012) 337-351.
- [44] P. Moser, A. Sallmann & I. Weisenberg, Synthesis and quantitative structure-activity relationships of diclofenac analogs, *J. Med. Chem.*, 33 (1990) 2358-2368.
- [45] A. Alvarez-Larena, J.F. Piniella, E. Carrasco, A. Ginebreda, S. Julia, & G. Germain, Crystal structure and spectroscopic study of 2-[(2,6-dichlorophenyl)amino]phenylacetoxyacetic acid (Aceclofenac), *J. Cryst. Spectroscopic Res.*, 22 (1992) 323-328.
- [46] G.R. Desiraju, & R. Parthasarathy, Cyano-halogen interactions and their role in the crystal structures of the 4-halobenzonitriles *J. Am. Chem. Soc.*, 111 (1989) 8725–8726.

- [47] V.A. Skoutakis, C.A. Carter, T.R. Mickle, V.H. Smith, C.R. Arkin, J. Alissandratos & D.E. Petty, Review of diclofenac and evaluation of its place in therapy as a nonsteroidal anti-inflammatory agent. *Drug Intell. Clin. Pharm.*, 22 (1988) 850-9.
- [48] C.R. Martinez, B.L. Iverson, Rethinking the term “pi-stacking” *Chemical Science*, 3 (2012) 2191-2201.
- [49] A. Katrusiak, Crystallographic autostereograms, *J. Mol. Graph. Model.* (2001),
- [50] J.J. McKinnon, M.A. Spackman & A.S. Mitchell, Novel tools for visualizing and exploring intermolecular interactions in molecular crystals. *Acta Crystallogr. B*, 60 (2004) 627–668.
- [51] M.A. Spackman, P.G. Byrom, A novel definition of a molecule in a crystal, *Chem. Phys. Lett.* 267 (1997) 215e220.
- [52] M.A. Spackman, From charge densities to crystal engineering, *Zeitschr. für Kristallogr.- Cryst. Mater.* 217 (2002).
- [53] C. Jelsch, K. Ejsmont, L. Huder, The enrichment ratio of atomic contacts in crystals, an indicator derived from the Hirshfeld surface analysis, *IUCr J.* 1, (2014) 119e128.
- [54] L.M. Salonen, M. Ellermann & F. Diederich, Aromatic rings in chemical and biological recognition: energetics and structures. *Angew. Chem. Int. Ed.* 50, (2011) 4808–4842.
- [55] C. Jelsch, S. Soudani, C. Ben Nasr, Atom interaction propensities of oxygenated chemical functions in crystal packings, *IUCr J.*, 2 (2015) 327-340.
- [56] P. Politzer, P. Lane, M.C. Concha, Y. Ma & J.S. Murray, An overview of halogen bonding, *J. Mol. Model.*, 13 (2007) 305–311.
- [57] M.E. Brezgunova, E. Aubert, S. Dahaoui, P. Fertey, S. Lebègue, C. Jelsch, & E. Espinosa, Charge Density Analysis and Topological Properties of Hal₃-Synthons and Their Comparison with Competing Hydrogen Bonds *Crystal Growth & Design*, 12 (2012) 5373-5386.
- [58] J. Galy, G. Couégnat, E. Vila & S.F. Matar, Stereochemistry of nitrogen lone pair in NH₃E, NO₂E, N₂O₃E₂, AgNO₂E, and NCl₃E *Comptes Rendus Chimie.* 20 (2017) 446-459.
- [59] M.A. Spackman, J.J. McKinnon & D. Jayatilaka, Electrostatic potentials mapped on Hirshfeld surfaces provide direct insight into intermolecular interactions in crystals. *Cryst. Eng. Comm.* 10, (2008) 377-388.
- [60] P. Sokkalingam, J. Shraberg, S. W. Rick, & B. C. Gibb. Binding hydrated anions with hydrophobic pockets. *J. Am. Chem. Soc.* 138 (2015). 48-51.

Table 1: Crystal and X-ray diffraction data collection details.

Chemical formula	C ₁₆ H ₁₃ Cl ₂ N O ₄
Formula weight (g.mol ⁻¹)	354.17
Crystal system, space group	Monoclinic, P 2 ₁ /n
<i>a</i> , <i>b</i> , <i>c</i> (Å)	12.1441(3), 8.2073(2), 15.3263(4)
<i>β</i> (°), <i>V</i> (Å ³)	95.053(2), 1521.64(7)
<i>Z</i>	4
Temperature (K)	100(1)
Radiation	Mo Kα, (λ = 0.71073 Å
Absorption coef. μ (mm ⁻¹)	0.45
Data collection method	Ωscans
Crystal #1 size (mm)	0.108 x 0.198 x 0.208 mm ³
Diffractometer #1	D8 VENTURE, microfocus source
<i>T</i> _{min} , <i>T</i> _{max}	multilayer mirror optic
Crystal #2 size (mm)	0.148 x 0.360 x 0.379 mm ³
Diffractometer #2	D8 QUEST standard sealed tube/graphite
<i>T</i> _{min} , <i>T</i> _{max}	0.8840, 0.9538
sinθ _{max} /λ (Å ⁻¹)	1.35
reflections measured #1 #2	922 215 , 880 311
independent reflections	30 891
<i>R</i> _{merge} (%)	4.06
WeightingschemeK [§]	3.082
<i>R</i> (<i>F</i>), <i>wR</i> ² (<i>I</i>) (%)	1.50, 1.77
Δρ min, max	-0.28 , +0.30
CCDC number	1936959

§ weighting scheme $W(I_{hkl}) = 1 / [K * \sigma(I_{obs})]^2$ applied to obtain goodness of fit $gof=1$.

Table 2: Geometry and topological properties of the hydrogen bonds, halogen bond and halogen...halogen interactions in the experimental charge density model. Distances are in Å, angles in degrees, electron density ρ_{cp} in $e/\text{Å}^3$ and Laplacian $\nabla^2\rho_{cp}$ in $e/\text{Å}^5$ (at the CPs). The symmetry operation applies to the third atom. X = hydrogen or halogen.

D-H...A	D-H	H...A	D...A	D-H...A	ρ_{cp}	$\nabla^2\rho_{cp}$
N1-H1...O4 ⁱ	1.006	2.130	3.02788(7)	147.58(2)	0.0927(16)	1.811(12)
C13-H13...CL2 ⁱⁱ	1.079	2.957	3.90907(13)	147.52(12)	0.0223(2)	0.362(5)
O2-H2...O1 ⁱⁱⁱ	0.973	1.865	2.6624(7)	137.26(16)	0.1650(18)	3.18(2)
C4-H4B...O1 ^{iv}	1.082	2.263	3.3388(11)	172.41(3)	0.0543(12)	1.408(9)
C4-H4B...O2 ⁱⁱ	1.082	2.595	3.1867(8)	113.65(10)	0.0497(4)	0.756(3)
C2-H2B...O4 ^v	1.088	2.280	3.35619(9)	169.65(5)	0.0558(13)	1.209(7)
X-B...A-Y		A...B	X-B...A	B...A-Y	ρ_{cp}	$\nabla^2\rho_{cp}$
C12-CL1...O4-C3 ⁱⁱ		3.08986(14)	165.895(1)	144.430(1)	0.0582(4)	0.805(8)
C12-CL1...CL2-C16 ⁱ		3.48775(10)	162.504(1)	104.403(3)	0.0451(2)	0.548(4)

Symmetry applies on acceptor atoms A. (i) $x ; y ; z$ (ii) $x ; y-1 ; z$ (iii) $-x+3/2 ; y+1/2 ; -z+3/2$ (iv) $-x+3/2 ; y-1/2 ; -z+3/2$ (v) $-x+1 ; -y+2 ; -z+1$

Table 3: Nature of contacts at the Hirshfeld surfaces: chemical content on the surface, proportion of contact types and contact enrichment ratios. Reciprocal contacts X-Y and Y-X were merged. The most abundant contacts C_{XY} are in bold characters. The enrichment values E_{XY} larger than unity are in bold and highlight enhanced interactions. Contribution of the N atoms, constituting 0.7% of the surface, is omitted. The non-polar and hydrophilic atoms have been regrouped.

atom	C	Hc	Cl	Hn/o	O
surface %	27.0	37.5	17.2	4.4	13.3
C	8.0	19.6	8.7	2.1	6.1
Hc		12.8	16.7	2.0	10.2
Cl			2.5	0.2	4.5
Hn/o	contacts (%)			0.0	5.1
O					0.1
C	1.16	0.99	0.94	0.85	0.89
Hc		0.90	1.26	0.58	1.04
Cl			0.83	0.09	0.98
Hn/o	enrichment			0.00	4.15
O					0.06

Table 4: Bader atomic charges(e) from theoretical and experimental refinements of ACF.

Atoms	Q_{theo}	Q_{exp}	Atoms	Q_{theo}	Q_{exp}
C1	1.54	1.55	H1	0.38	0.42
C2	0.35	0.31	H2	0.13	0.62
C3	1.45	1.42	H2A	0.09	0.09
C4	0.03	-0.04	H2B	0.13	0.18
C5	0.03	-0.05	H4A	0.05	0.07
C6	-0.02	0.00	H4B	0.09	0.09
C7	-0.02	-0.28	H6	0.05	0.06
C8	-0.02	0.01	H7	0.05	0.11
C9	-0.01	-0.12	H8	0.05	0.07
C10	0.3	0.34	H9	0.04	0.11
C11	0.38	0.38	H13	0.06	0.18
C12	0.02	-0.01	H14	0.07	0.19
C13	0.01	-0.01	H15	0.09	0.14
C14	-0.02	-0.12	O1	-0.99	-1.16
C15	0.02	-0.03	O2	-1.12	-1.08
C16	0.02	0.12	O3	-0.91	-1.06
CL1	-0.14	-0.18	O4	-1.12	-1.15
CL2	-0.17	-0.16	N1	-0.92	-1.00

Table 5. Electrostatic energy (kJ/mol) between interacting dimers in the crystal. Dimers related by an involutory symmetry (*) are given a coefficient $\frac{1}{2}$ in the summation, as the other symmetry operators σ account for two dimers: ACF... σ (ACF) and ACF... σ^{-1} (ACF).

symmetry	$-E_{\text{elec}}$	Main contacts
$\frac{3}{2}-x, -\frac{1}{2}+y, \frac{3}{2}-z$	66.8	two O-H...O
$-x, 1-y, 1-z$ (*)	28.5	C ₆ Cl ₂ stacking
$1-x, 2-y, 1-z$ (*)	25.2	Twice O4...H2B-C2
$1-x, 1-y, 1-z$ (*)	19.2	C-H...N ; Cl...C
$\frac{1}{2}+x, \frac{1}{2}-y, \frac{1}{2}+z$	11.2	π ...H-C
$-\frac{1}{2}+x, \frac{3}{2}-y, -\frac{1}{2}+z$	10.3	COOH / C ₆ Cl ₂ stacking
$\frac{1}{2}-x, -\frac{1}{2}+y, \frac{3}{2}-z$	4.3	H7...Cl2
$x, y-1, z$	1.0	CL1...O4
total	130.0	

Table 6. Electrostatic interaction E_{elec} energies (kJ.mol⁻¹) between Diclofenac and residues in the cyclooxygenase-2 active site (PDB code 1PXX). The E_{elec} values are averaged over the four monomers of COX2/diclofenac complexes found in the asymmetric unit and the sample standard deviations are also given between parentheses. Values are calculated for protonated (COOH) and non-protonated (COO⁻) forms of diclofenac.

Residue	COOH	COO ⁻	Residue	COOH	COO ⁻
Tyr 385	-60(16)	-86(25)	Leu 384	-2.1(5)	-20(5)
Ser 530	-52(14)	-30(18)	Phe 381	-8.2(2)	-16(1)
Leu 531	4(3)	-34(2)	Val 349	-15(2)	-43(2)
Ala 527	1(2)	9(1)	Phe 518	-3.4(5)	-7(1)
Tyr 355	1(9)	3(1)	Val 523	-6.9(3)	-15(2)
Ser 353	-1(3)	-2(2)	Phe 205	-3.5(1)	-13(1)
Tyr 348	-6(1)	-3(1)	Met 522	-5.5(8)	9(1)
Gly 526	-8(6)	3(6)	Leu 352	-11(1)	-30(2)
Trp 387	-12(2)	-30(2)	Total	-186(23)	-305(25)

Table 7. Hirshfeld surface content on the protein/ligand interface, followed by the actual contacts $C_{xy}(\%)$ and their enrichments E_{xy} . The values were averaged over the four molecules in the asymmetric unit and sample standard deviations are shown between parentheses. The S and N atoms related to small surface areas are omitted. The hydrogen atoms bound to carbon (Hc) are distinguished from the more polar H atoms bound to O or N (Ho/n). The Q species relates to no chemical species assigned to the surface and corresponds to protein regions of very small electron density (empty cavity or non-modelled solvent molecule). The major contacts and most enriched ones are in bold.

Protein		Ho/n	O	C	Hc	Q
Surface %		8.3(4)	6.2(4)	10.0(3)	67.9(4)	5.7(5)
C_{xy} ligand	Ho/n	0.3(1)	1.5(2)	0.58(2)	3.43(3)	0.3(1)
	O	3.8(2)	0.24(6)	0.3(2)	3.81(3)	0.29(8)
	C	0.47(3)	0.2(2)	3.0(2)	22.97(4)	1.5(3)
	Hc	3.73(5)	3.76(5)	5.4(1)	19.1(2)	2.5(2)
	Cl	0	0.59(3)	0.75(7)	18.22(4)	1.3(1)
E_{xy} ligand	Ho/n	0.67(3)	3.96(4)	0.94(3)	0.83(5)	0.7(3)
	O	5.43(3)	0.5(1)	0.3(2)	0.67(5)	0.6(2)
	C	0.2(2)	0.09(7)	1.06(5)	1.19(2)	0.9(1)
	Hc	1.3(2)	1.7(2)	1.51(7)	0.79(1)	1.2(2)
	Cl	0	0.46(2)	0.36(4)	1.29(3)	1.05(5)
Ligand	Ho/n	O	C	Hc	Cl	
Surface %		6.1(1)	8.4(3)	28.5(2)	35.7(3)	20.8(1)

Figures

Figure 1: ORTEP view of ACF molecule, showing the atom-numbering scheme. Displacement ellipsoids are drawn at the 50% probability level.

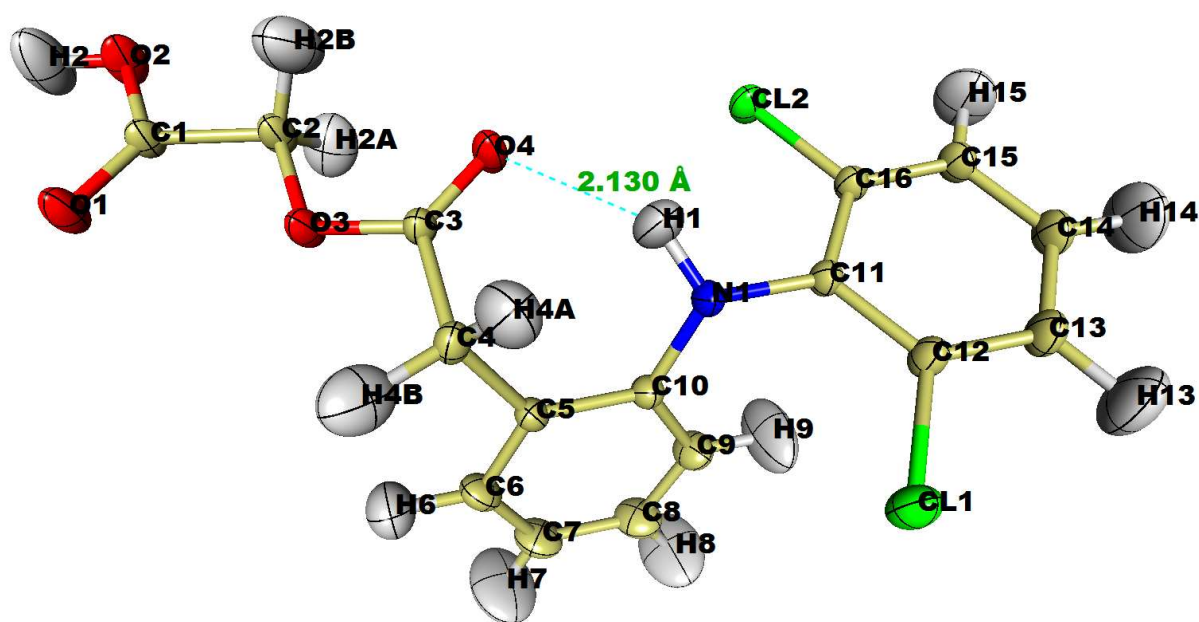
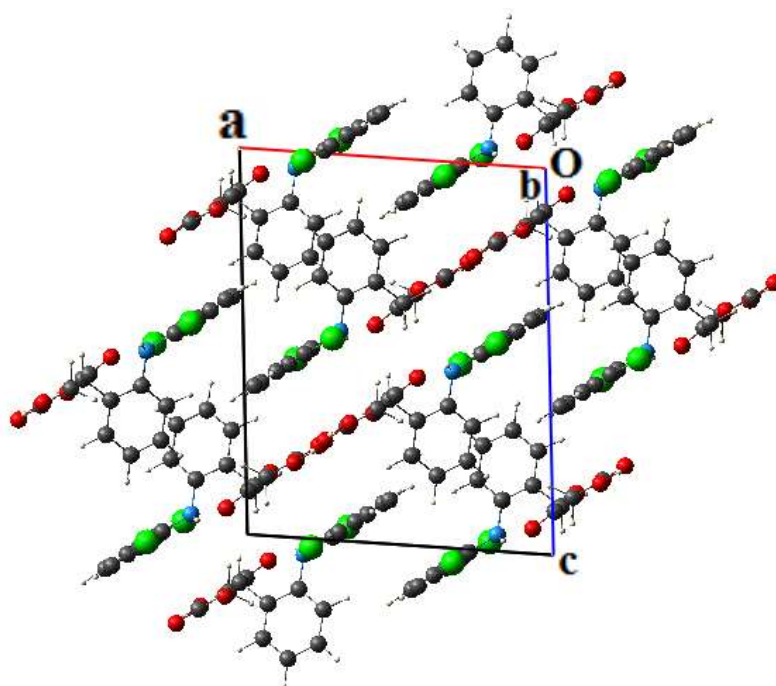
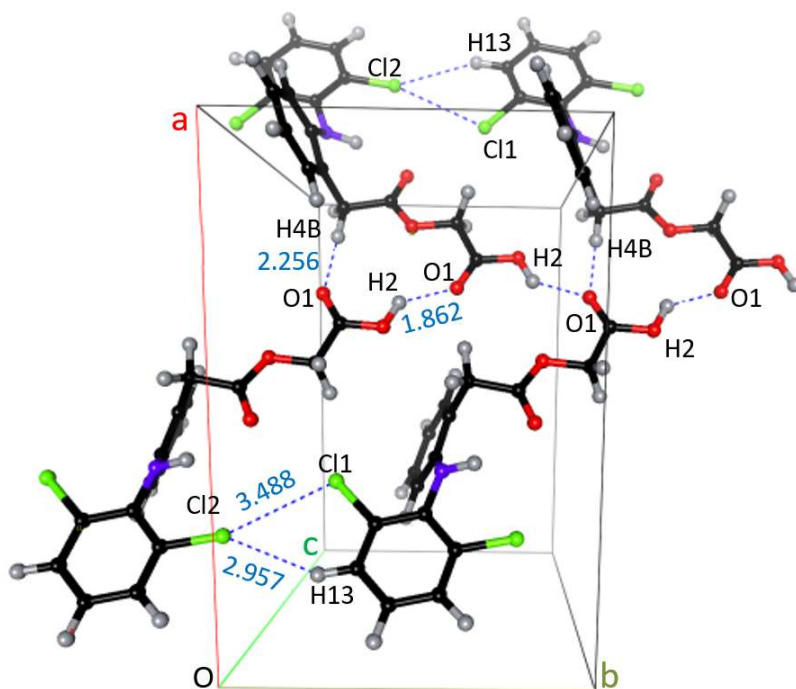


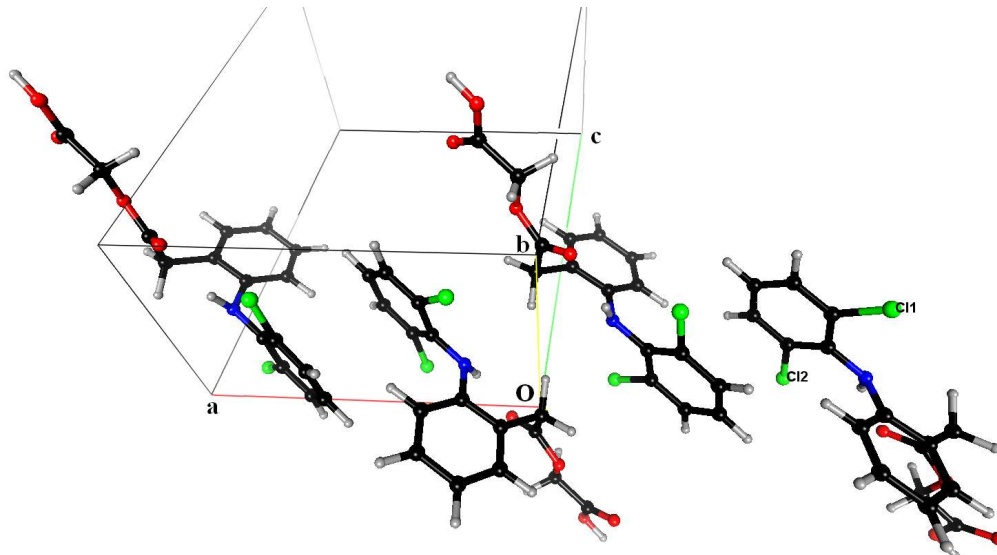
Figure 2: (a) View of the crystal packing of ACF shown along the **b** axis



(b) Auto-stereogram [49] showing the chain along the **b** axis of $O1 \cdots H2$ hydrogen bonds between terminal carboxylic acid groups.



(c) Auto-stereogram showing stacking between two dichlorobenzene rings related by inversion centre.



(d) View of the dimer related by an inversion center with a double hydrogen bond between the C=O ester group and C15-H15B. Symmetry operation: $(2-x, 2-y, -z)$.

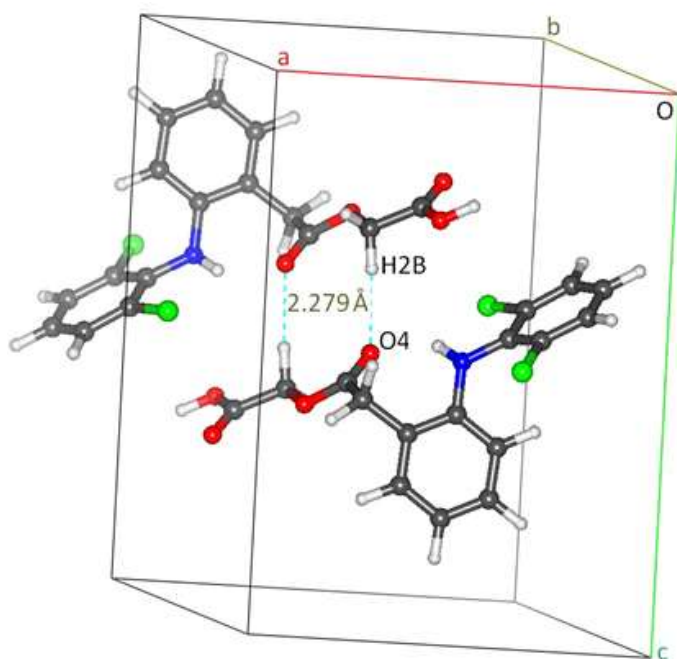
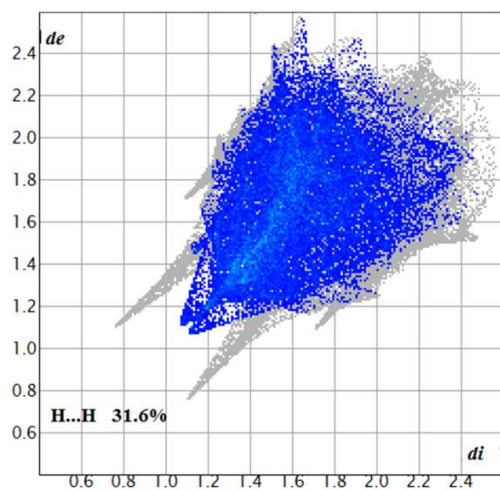


Figure 3: Fingerprint plots of the contacts on the ACF crystal Hirshfeld surface (a) H...H and (b) O...H/H...O contacts.

a)



b)

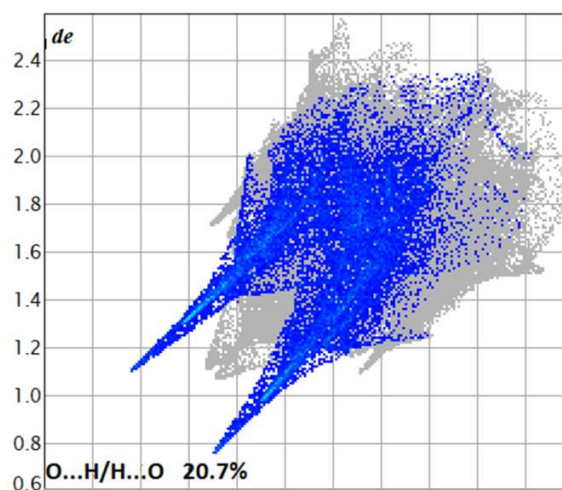


Figure 4: Superposition of ACF experimental geometry structure (carbon as gray sticks) and isolated molecule (carbon as pink sticks). Superposition is done on the central phenyl ring atoms.

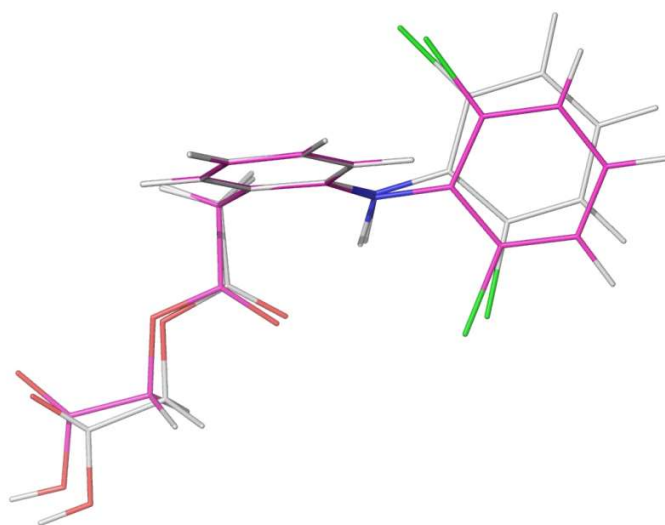
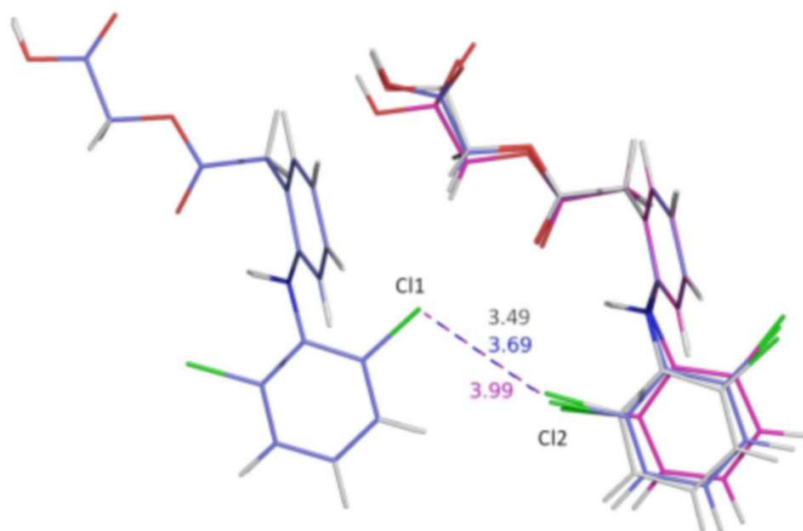


Figure 5: Superposition of ACF dimer consisting of two molecules related by **b** axis translation. +**b** direction is towards the left. Experimental geometry structure: carbon in gray; optimized molecule with the dimer: carbon and distances in blue; optimized isolated molecule: carbon and distances in pink. Selected inter-atomic distances are given in Å.

(a) The molecule on the left was kept fixed while the one on the right was optimized. **b** vector is directed towards the right



(b) The molecule on the right was kept fixed while the one on the left was optimized.

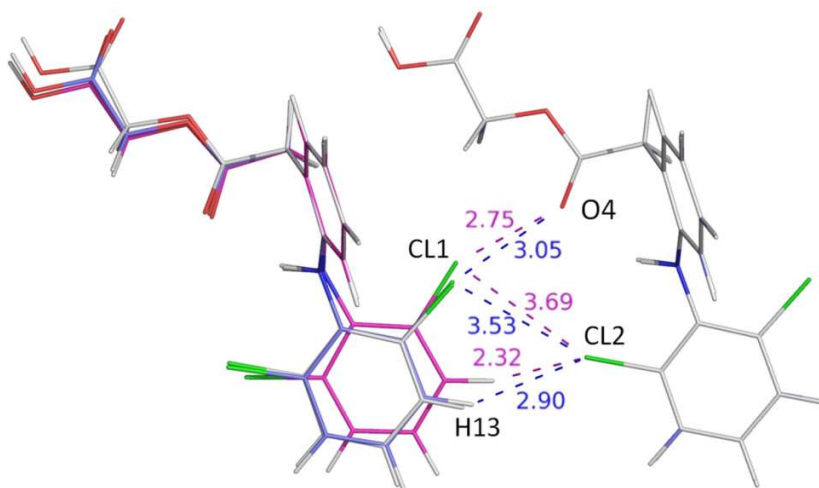
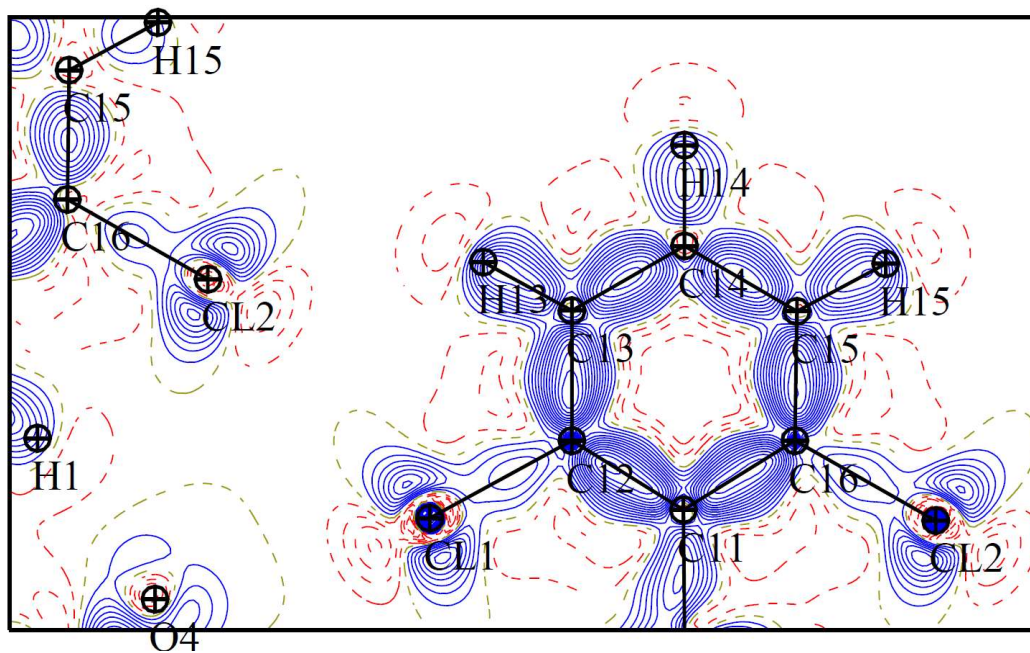
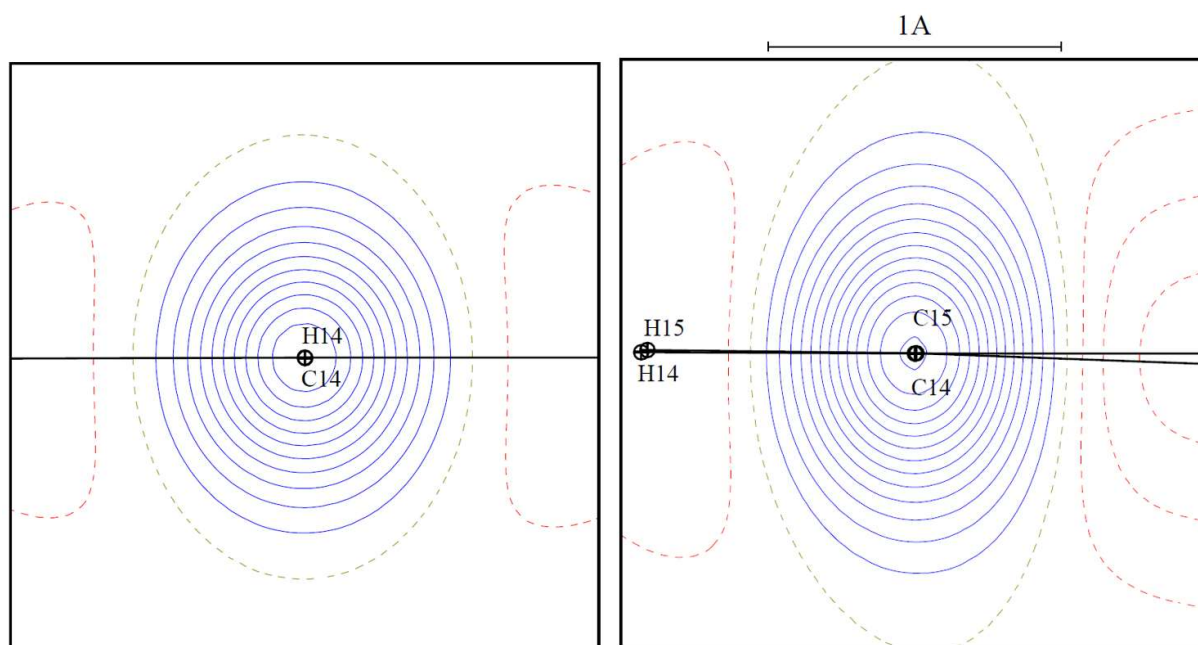


Figure 6: Static deformation electron density maps computed from experimental charge density. Contour intervals are $0.05 \text{ e}\text{\AA}^{-3}$; blue lines represent positive contours, red lines are negative contours and the green lines are zero contours.

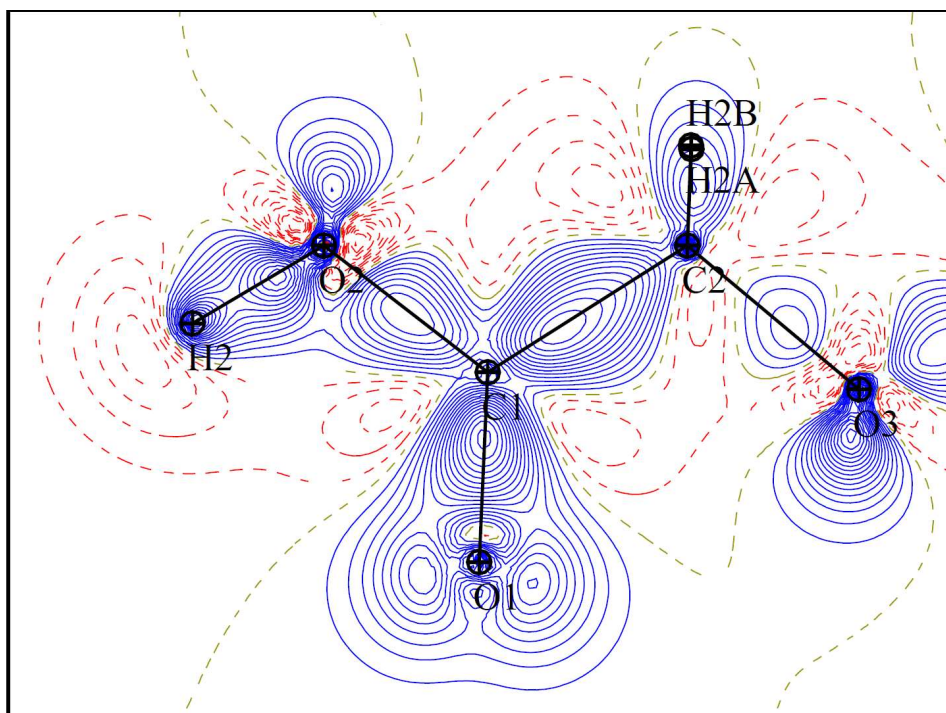
(a) in the dichlorophenyl plane,



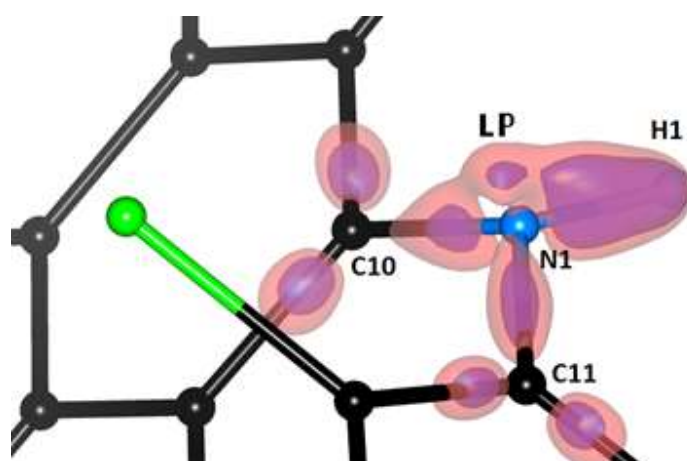
(b) in the planes containing the critical points of the C14-H14 and C14-C15 bonds and perpendicular to these bonds



(c) in the ester C2-O2-C1 plane.



(d) 3D map around the N1 atom. Outer (red) and inner (blue) iso-surfaces are of values $+0.25$ and $+0.4 \text{ e}/\text{\AA}^3$, respectively.



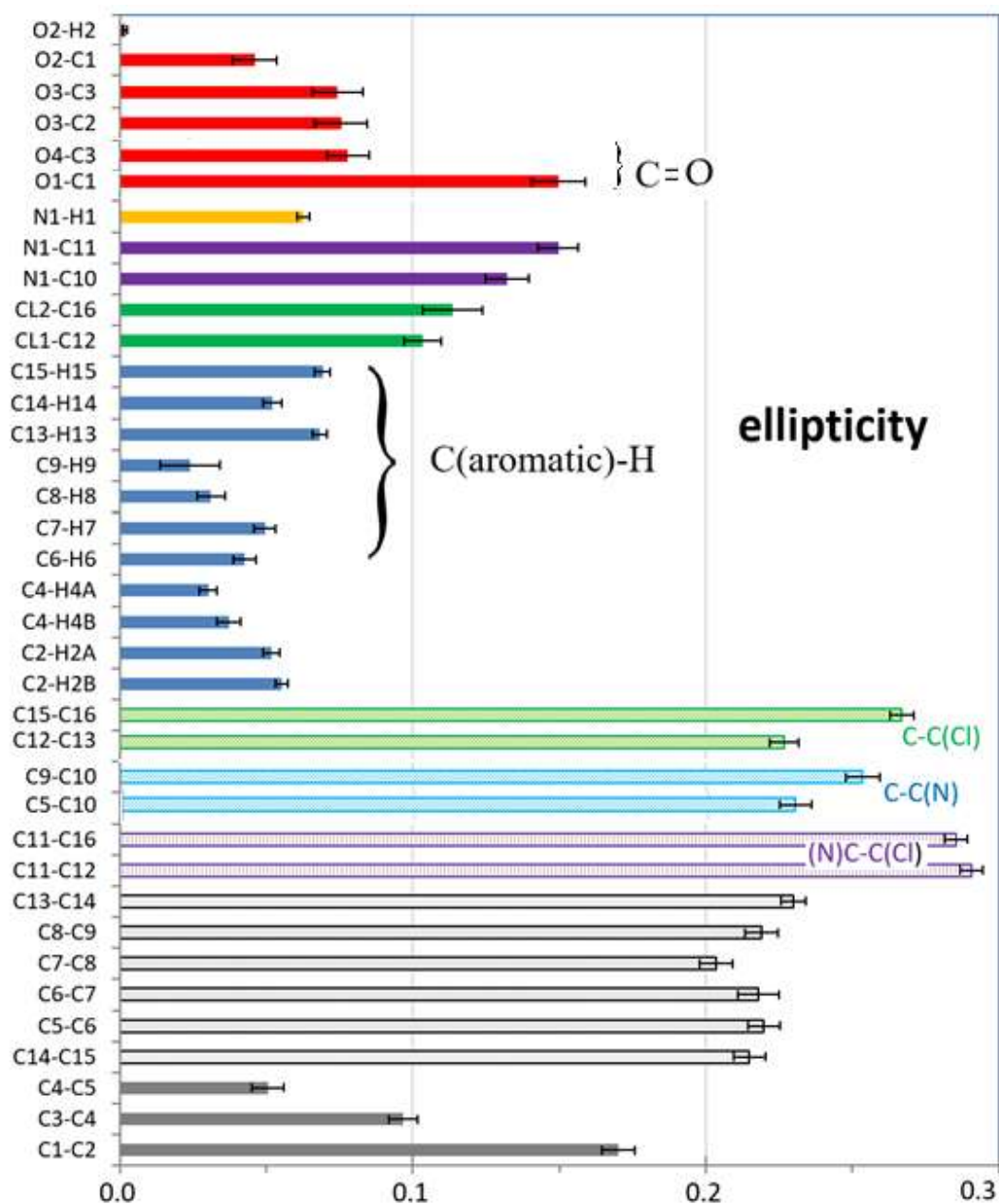


Figure 7: Ellipticity at the covalent bond CPs. Error bars are obtained from the sample standard deviation method. The C-C simple bonds are in grey. The C-C aromatic bonds with a carbon atom bound to Cl or N are highlighted in color.

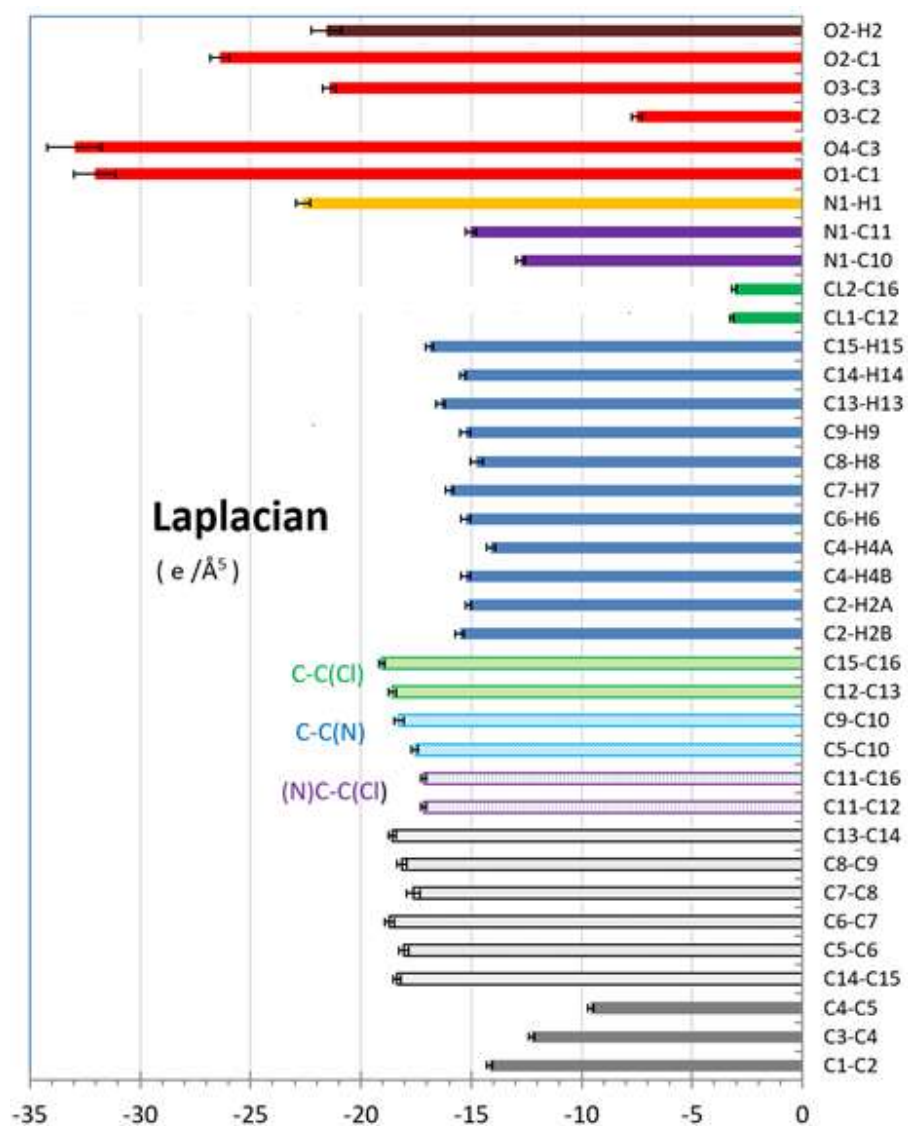
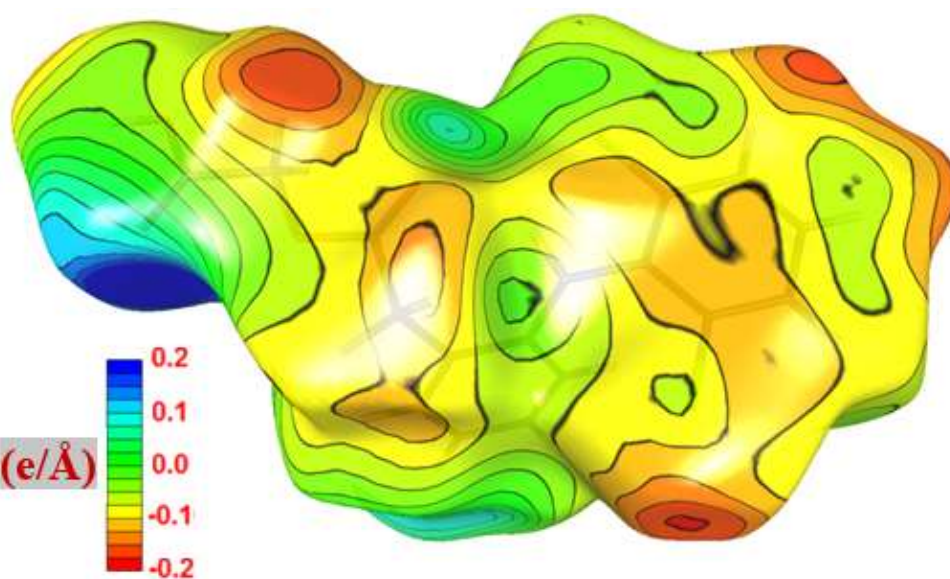
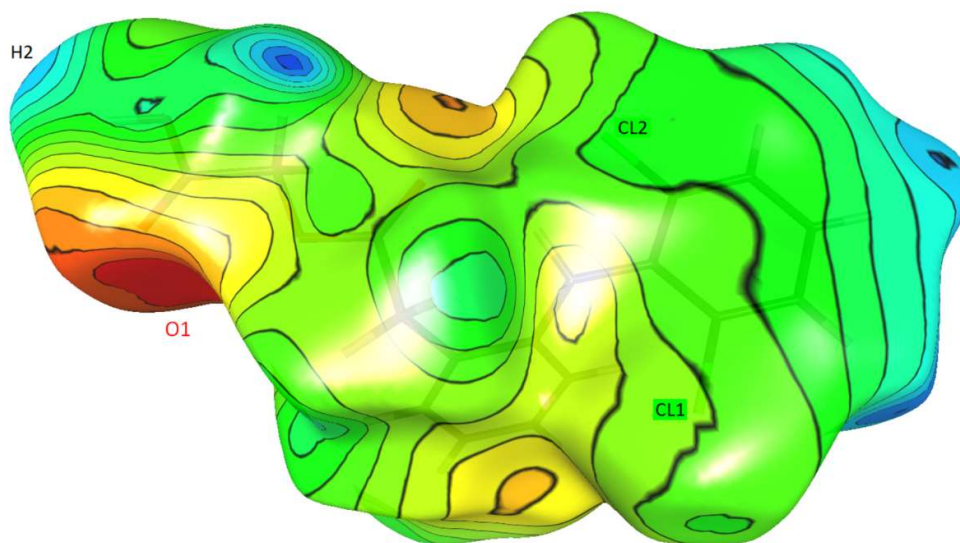


Figure 8: Laplacian at the covalent bond CPs. Colors of bond types are the same as in Fig. 7.

Figure 9: Hirshfeld surface colored according to the Electrostatic Potential value.

(a) generated by ACF molecule. (b) generated by a cluster of 13 molecules surrounding the asymmetric unit. Orientation is the same as in Fig. 1. Symmetry codes: $x;y-l;z$, $x;y+l;z$, $-x+\frac{3}{2};y-\frac{1}{2};-z+\frac{1}{2}$, $-x+\frac{3}{2};y+\frac{1}{2};-z+\frac{1}{2}$, $-x+\frac{5}{2};y-\frac{1}{2};-z+\frac{1}{2}$, $-x+\frac{5}{2};y+\frac{1}{2};-z+\frac{1}{2}$, $-x+l;-y+l;-z$, $-x+2;-y+l;-z$, $-x+2;-y+2;-z$, $x-\frac{1}{2};-y+\frac{1}{2};z-\frac{1}{2}$, $x-\frac{1}{2};-y+\frac{3}{2};z-\frac{1}{2}$, $x+\frac{1}{2};-y+\frac{1}{2};z+\frac{1}{2}$, $x+\frac{1}{2};-y+\frac{3}{2};z+\frac{1}{2}$

a)



b)

Figure 10: Scatterplot of the electrostatic potential $V_{\text{int}}(\mathbf{r})$ vs. $V_{\text{ext}}(\mathbf{r})$ on the Hirshfeld surface of ACF molecule. The external potential $V_{\text{ext}}(\mathbf{r})$ is generated by 13 neighboring ACF molecules, as in Fig. 9b. The (H...O) and (H...Cl) hydrogen bonds are highlighted in the graph. A square root scale has been used for better visualization.

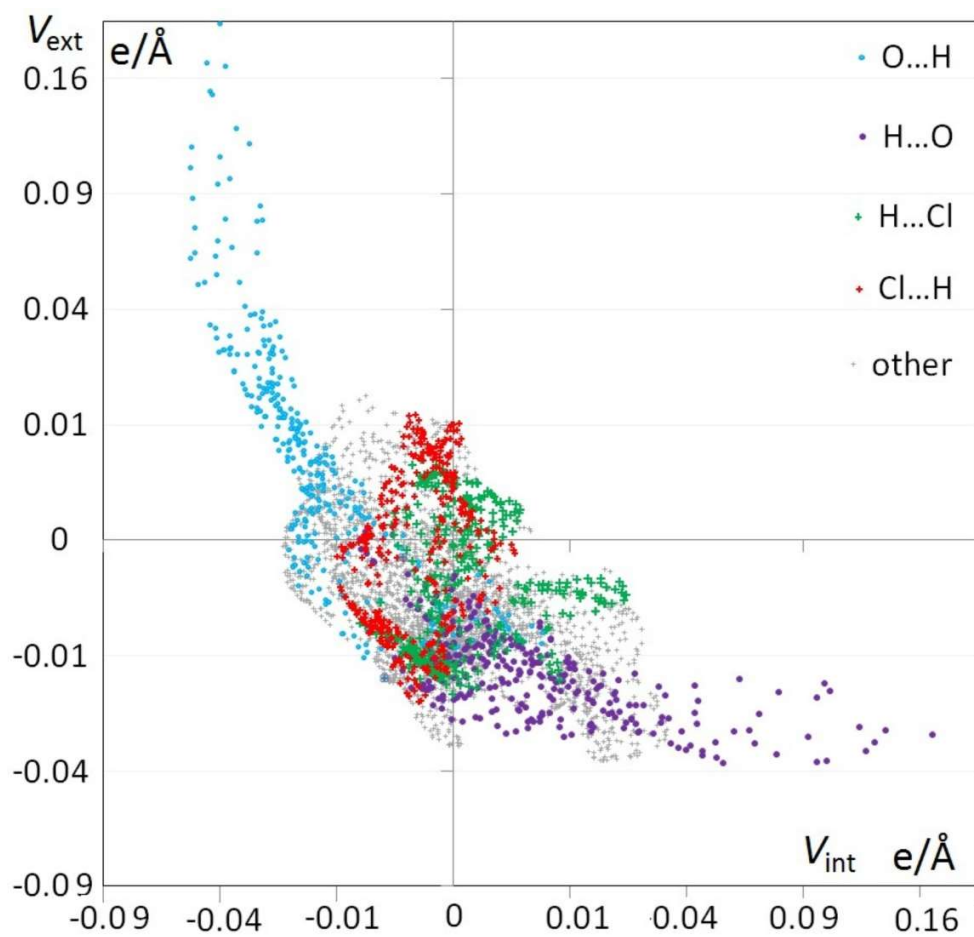
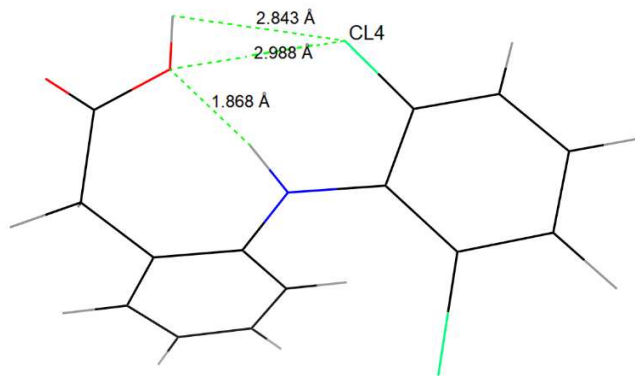
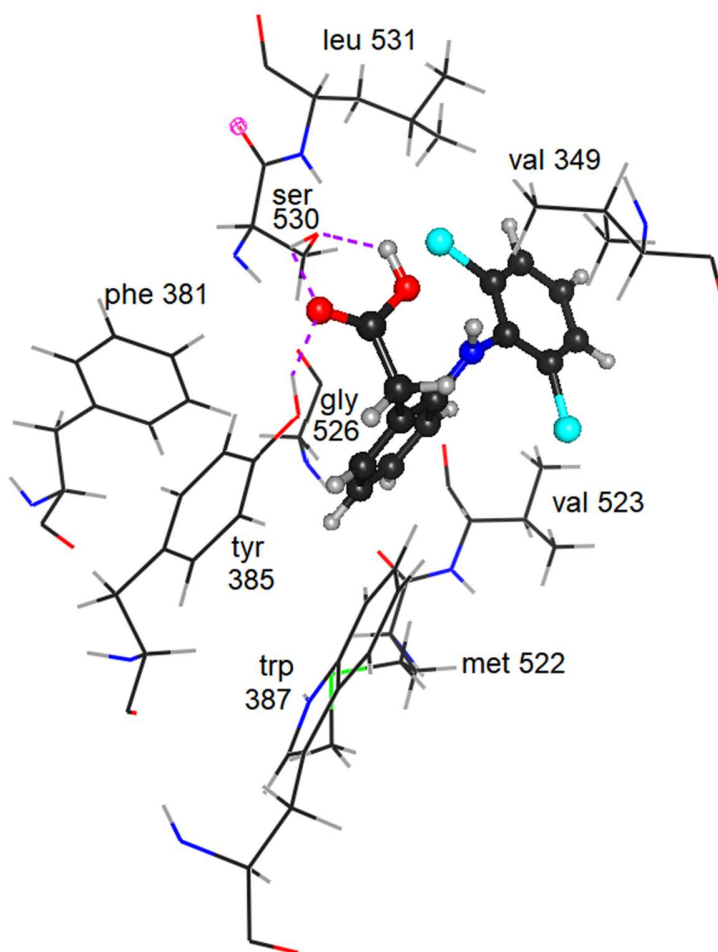


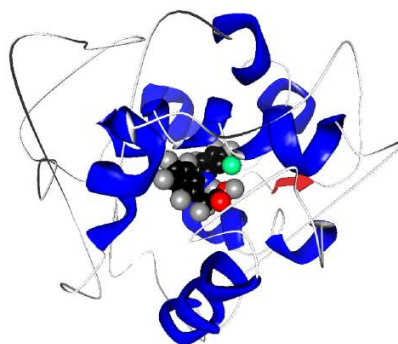
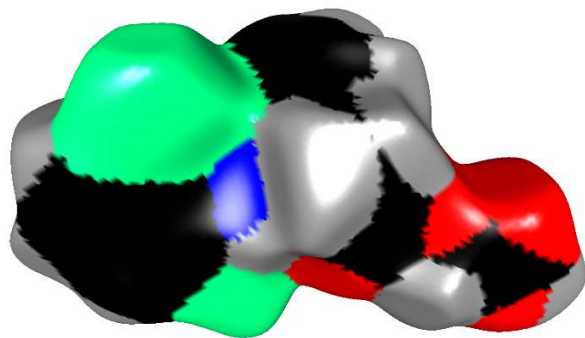
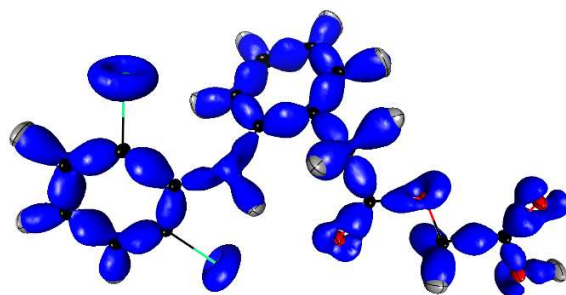
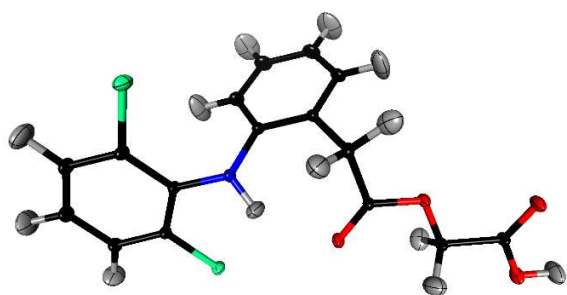
Figure 11: (a) Conformation of Diclofenac molecule in monomer #1 of COX2/DCF complex with important intramolecular distances..



b) View of the interactions of the DCF drug with the COX2 protein active site residues.



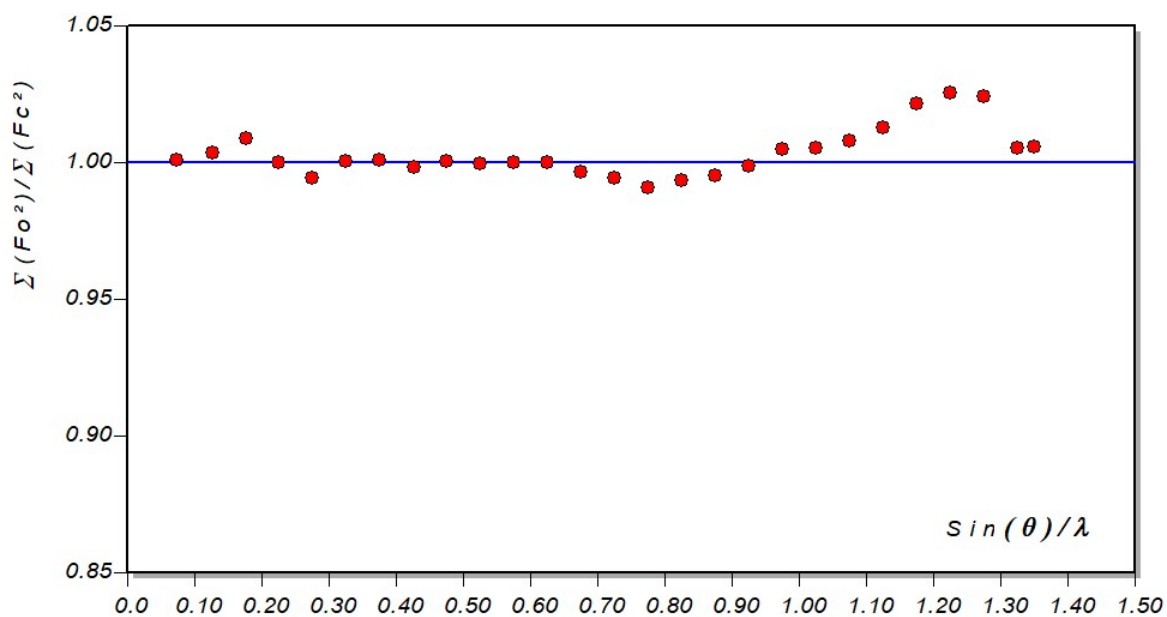
Graphical Abstract.



Supplementary Materials.

Figure S1: Variation of scale factor, $\Sigma(Fo^2)/\Sigma(Fc^2)$ with respect to resolution, obtained using program DRKplot (Zhurov, Zhurova& Pinkerton, J. Appl. Cryst. (2008). 41, 340–349).

(a) Experimental



(b) Theoretical up to $s < 1 \text{ \AA}^{-1}$

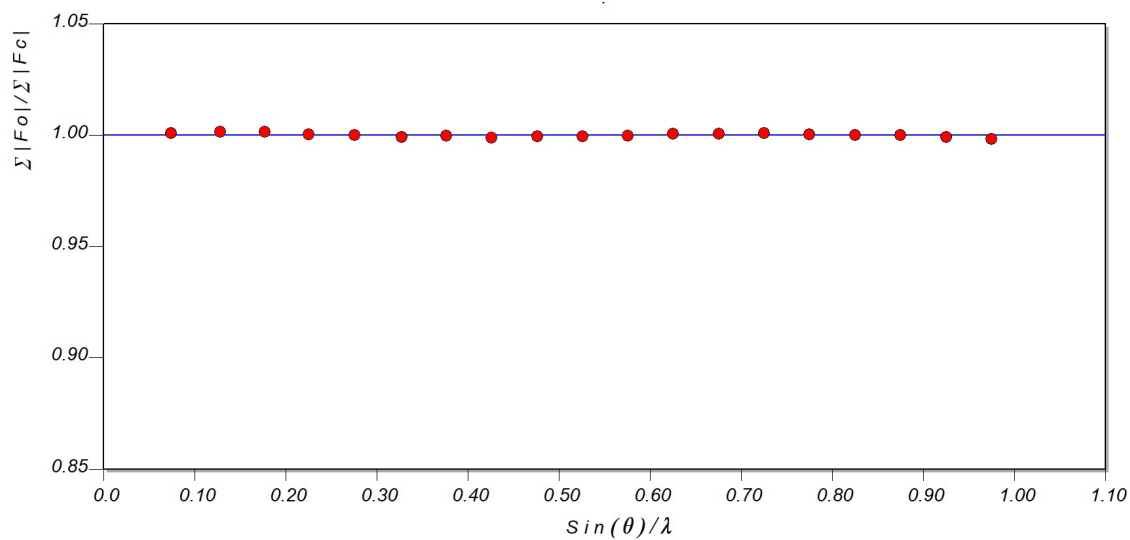
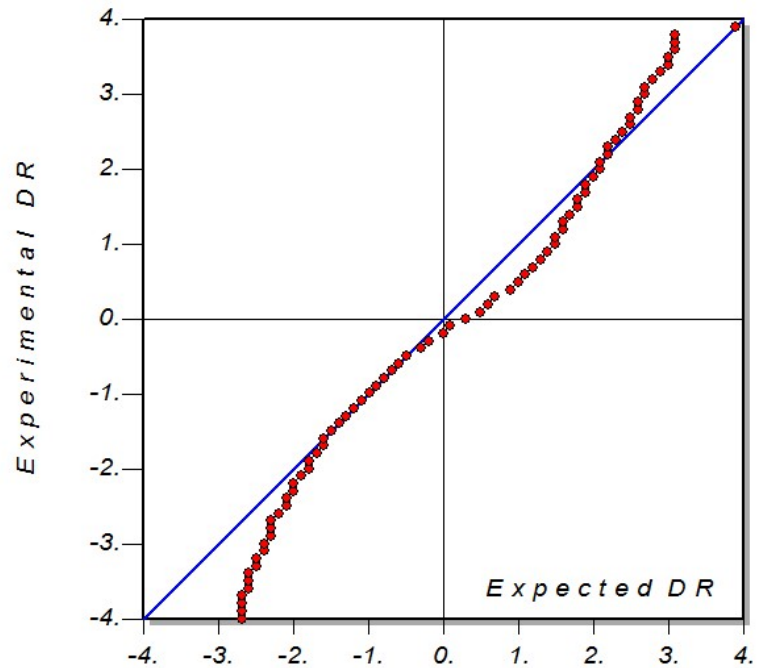


Figure S2: Normal probability plot of $(F^2_o - F^2_c)$ using program DRKplot (Zhurov, Zhurova & Pinkerton, J. Appl. Cryst. (2008). 41, 340–349).

(a) Experimental.

Weighting scheme used:

$$W = 9.5 / [\sigma(F^2)]^2.$$



(b) Theoretical

F_{hkl} data at $s < 1 \text{ \AA}^{-1}$
 $gof = 1$ is achieved
 when applying
 $\sigma(F) = 0.092$

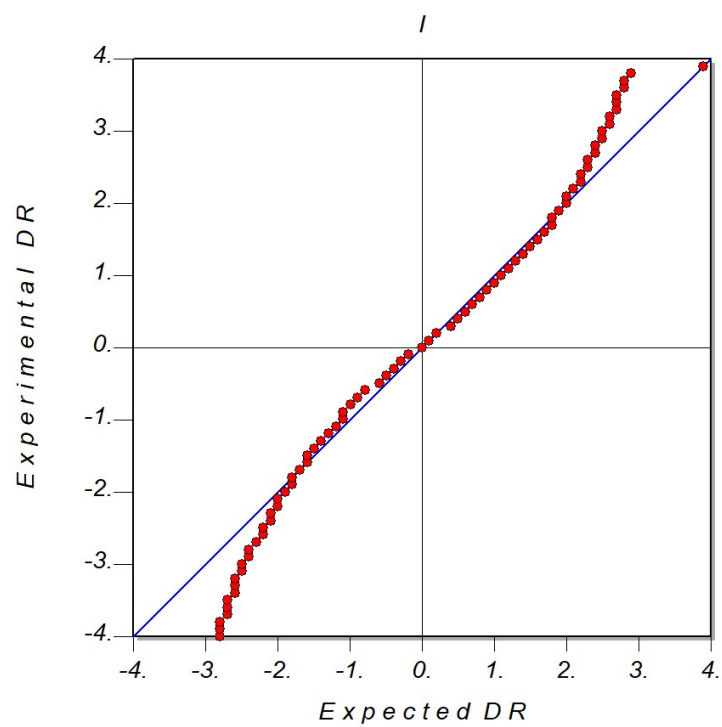
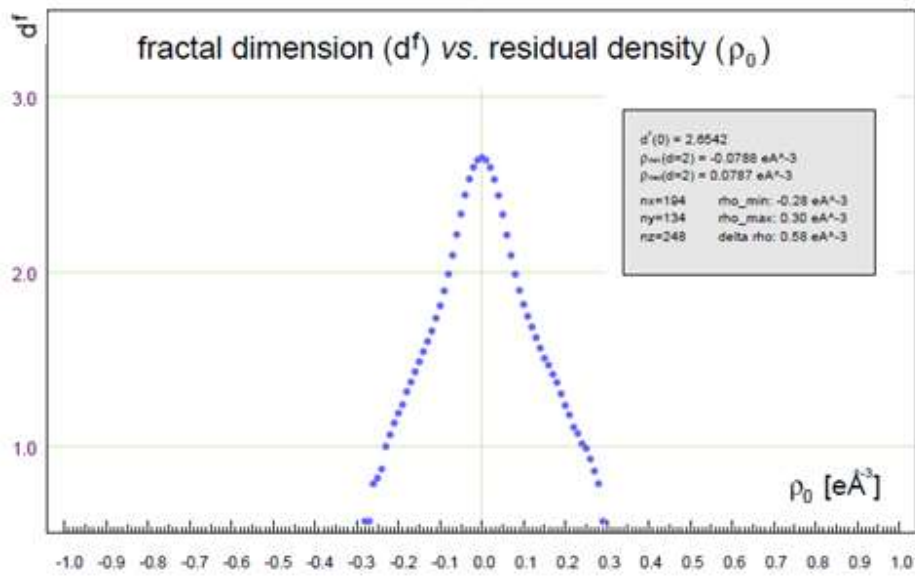


Figure S3. Fractal dimension vs. residual electron density F_o-F_c
(Meindl, K & Henn, J., *Acta Crystallogr.*(2008). A64, 404-418)

(a) Experimental, using all reflections.



(b) Theoretical at $s < 1\text{\AA}^{-1}$

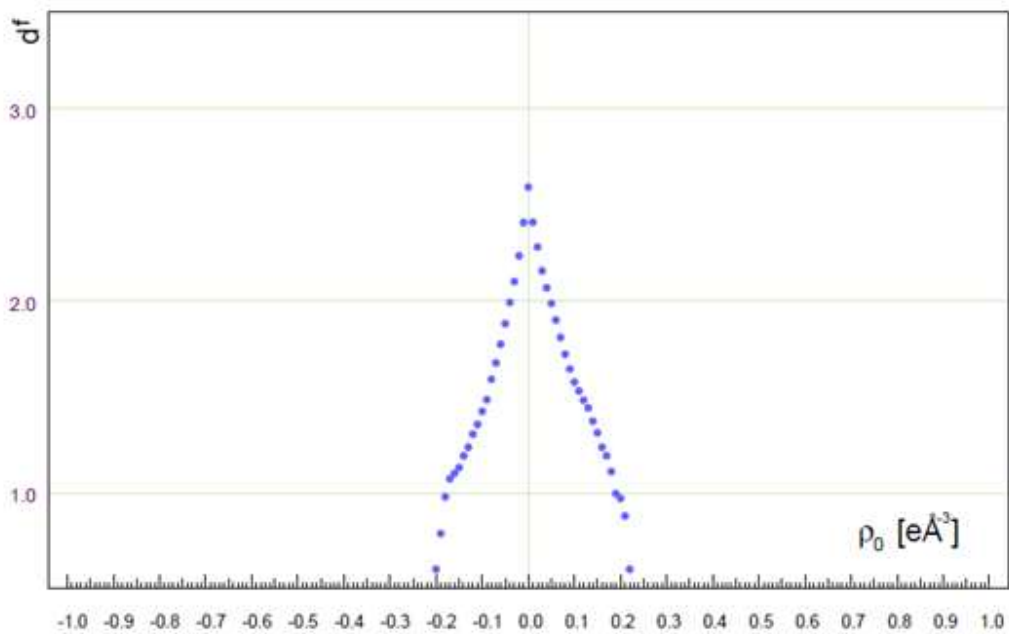


Table S1: Topological properties at the covalent bond critical points: ρ electron density ($e/\text{\AA}^3$), $-\text{Laplacian}\nabla^2\rho$ ($e/\text{\AA}^5$), ellipticity, and their uncertainties estimated by the sample standard deviation method.

bond	ρ	$ssd(\rho)$	Laplacian	$ssd(\Delta\rho)$	ϵ	$ssd(\epsilon)$
C1-C2	1.8178	0.0066	-14.32	0.20	0.1687	0.0061
C3-C4	1.7511	0.0071	-12.03	0.19	0.1009	0.0070
C4-C5	1.6656	0.0045	-9.49	0.17	0.0534	0.0054
C5-C10	2.1163	0.0075	-17.65	0.25	0.2258	0.0072
C5-C6	2.1397	0.0050	-18.26	0.21	0.2304	0.0100
C6-C7	2.1926	0.0071	-18.58	0.29	0.2300	0.0086
C7-C8	2.1405	0.0062	-16.55	0.31	0.2018	0.0094
C8-C9	2.1616	0.0071	-18.13	0.20	0.2054	0.0063
C9-C10	2.1366	0.0061	-18.09	0.21	0.2531	0.0043
C11-C12	2.0900	0.0067	-17.14	0.22	0.2957	0.0062
C11-C16	2.0711	0.0062	-17.38	0.21	0.2898	0.0066
C12-C13	2.1689	0.0063	-18.59	0.24	0.2268	0.0040
C13-C14	2.1614	0.0059	-18.56	0.22	0.2297	0.0079
C14-C15	2.1522	0.0071	-18.37	0.17	0.2149	0.0077
C15-C16	2.1511	0.0045	-19.06	0.19	0.2668	0.0059
C2-H2B	1.8050	0.0078	-15.92	0.24	0.0667	0.0038
C2-H2A	1.8249	0.0086	-14.68	0.27	0.0412	0.0049
C4-H4B	1.8391	0.0061	-15.82	0.20	0.0413	0.0047
C4-H4A	1.7760	0.0075	-14.16	0.22	0.0299	0.0067
C6-H6	1.8072	0.0071	-15.90	0.21	0.0656	0.0039
C7-H7	1.9154	0.0059	-16.04	0.29	0.0405	0.0038
C8-H8	1.8552	0.0073	-15.31	0.28	0.0360	0.0040
C9-H9	1.9053	0.0067	-15.29	0.29	0.0266	0.0125
C13-H13	1.7986	0.0098	-15.67	0.24	0.0709	0.0049
C14-H14	1.8047	0.0064	-15.59	0.27	0.0480	0.0045
C15-H15	1.8587	0.0059	-16.61	0.23	0.0664	0.0029
CL1-C12	1.3562	0.0061	-3.40	0.20	0.0949	0.0104
CL2-C16	1.3124	0.0066	-2.75	0.17	0.1317	0.0106
N1-C10	1.9629	0.0098	-12.84	0.28	0.1263	0.0078
N1-C11	2.0659	0.0072	-15.39	0.20	0.1522	0.0087
N1-H1	2.1928	0.0123	-23.07	0.41	0.0634	0.0020
O1-C1	2.9938	0.0112	-29.59	1.33	0.1750	0.0094
O2-C1	2.2947	0.0094	-26.61	0.51	0.0460	0.0080
O3-C2	1.6586	0.0064	-7.52	0.26	0.0866	0.0107
O3-C3	2.1741	0.0068	-22.12	0.26	0.0825	0.0087
O4-C3	3.0243	0.0080	-31.42	1.00	0.0844	0.0062
O2-H2	2.2086	0.0134	-22.70	0.71	0.0003	0.0009

Table S2. . List constraints and restraints applied.

Constraints

```

SYMPLM my    O2  1  0.01
SYMPLM my    O3  1  0.01

FIXUIJ H13   1  0.034545  0.016150  0.043135  -0.006187  -0.005449  -0.003540
FIXUIJ H14   1  0.024758  0.033140  0.037688  -0.007513  -0.013307  -0.003190
FIXUIJ H15   1  0.025708  0.026474  0.034078   0.005573  -0.008764   0.005122
FIXUIJH6    1  0.030429  0.062827  0.026295  -0.013242  -0.010552   0.003527
FIXUIJH7    1  0.050250  0.074464  0.016884  -0.007185   0.000285   0.010886
FIXUIJH8    1  0.038411  0.073744  0.034766  -0.016554   0.012861   0.016795
FIXUIJH9    1  0.023984  0.066192  0.034820  -0.020128  -0.002286   0.007239
FIXUIJH1    1  0.028212  0.019286  0.031091  -0.008704  -0.007272   0.008475
FIXUIJH2    1  0.025406  0.019166  0.037280  -0.001088  -0.010761  -0.000989
FIXUIJH2A   1  0.024139  0.025584  0.038709   0.002633   0.002994  -0.004811
FIXUIJH2B   1  0.037023  0.025514  0.023913  -0.003643  -0.002514   0.004372
FIXUIJH4A   1  0.021839  0.026536  0.031882  -0.000370  -0.005447   0.005799
FIXUIJH4B   1  0.035856  0.023541  0.021933  -0.002447   0.003389  -0.002921

```

Restraints

```

! PREP REST KAPP
SIMKAP CL1   1  CL2   1  0.003
SIMKAP C12   1  C16   1  0.003
SIMKAP C13   1  C15   1  0.003
SIMKAP H2A   1  H2B   1  0.003
SIMKAP H4A   1  H4B   1  0.003
SIMKAP H6    1  H7    1  H8    1  H14   1  0.003
SIMKAP H13   1  H15  1  0.003

```

```

! PREP RES EQUI
SIMPLM 1 CL1 CL2 0.003
SIMPLM 1 C12 C16 0.003
SIMPLM 1 C13 C15 0.003
SIMPLM 1 O1 O4 0.003
SIMPLM 1 C6 C14 0.003

```

```

! PREP RES SYMP
RSYMUL mxmy CL1 1 0.003
RSYMUL mxmy CL2 1 0.003
RSYMUL mz O1 1 0.003
RSYMUL mz O4 1 0.003
RSYMUL mx N1 1 0.003
RSYMUL mz C1 1 0.003
RSYMUL my C2 1 0.003
RSYMUL mz C3 1 0.003
RSYMUL mxmy C4 1 0.003
RSYMUL mymz C5 1 0.003
RSYMUL mymz C6 1 0.003

```

```

RSYMUL mymz      C7      1      0.003
RSYMUL mymz      C8      1      0.003
RSYMUL mymz      C9      1      0.003
RSYMUL mz        C10     1      0.003
RSYMUL mymz      C11     1      0.003
RSYMUL mymz      C12     1      0.003
RSYMUL mymz      C13     1      0.003
RSYMUL mymz      C14     1      0.003
RSYMUL mymz      C15     1      0.003
RSYMUL mymz      C16     1      0.003

SIMPLM  1  H2A    H2B    0.003
SIMPLM  1  H4A    H4B    0.003
SIMPLM  1   H6    H14    0.003
SIMPLM  1  H13    H15    0.003
SIMPLM  1  H4A    H13    0.003

SIMK12  CHEM  H  0.003

RESKP1  CHEM  C1  0.999718  0.001

! PREP REST SIMD
SIMDIS  1  C11  H1  C10  H1  0.01
SIMDIS  1  C2  H2B  C2  H2A  0.01
SIMDIS  1  O3  H2B  O3  H2A  0.01
SIMDIS  1  C1  H2B  C1  H2A  0.01
SIMDIS  1  C4  H4A  C4  H4B  0.01
SIMDIS  1  C3  H4A  C3  H4B  C5  H4A  C5  H4B  0.01
SIMDIS  1  C5  H6  C7  H6  0.01
SIMDIS  1  C6  H7  C8  H7  0.01
SIMDIS  1  C9  H8  C7  H8  0.01
SIMDIS  1  C10 H9  C8  H9  0.01
SIMDIS  1  C12 H13 C14 H13 0.01
SIMDIS  1  C15 H14 C13 H14 0.01
SIMDIS  1  C16 H15 C14 H15 0.01

! PREP REST DIST
DISTAN  O2  1      H2  1      0.980  0.002
DISTAN  N1  1      H1  1      1.015  0.002
DISTAN  C2  1      H2B 1      1.092  0.002
DISTAN  C2  1      H2A 1      1.092  0.002
DISTAN  C4  1      H4A 1      1.092  0.002
DISTAN  C4  1      H4B 1      1.092  0.002
DISTAN  C6  1      H6  1      1.083  0.002
DISTAN  C7  1      H7  1      1.083  0.002
DISTAN  C8  1      H8  1      1.083  0.002
DISTAN  C9  1      H9  1      1.083  0.002
DISTAN  C13 1      H13 1      1.083  0.002
DISTAN  C14 1      H14 1      1.083  0.002
DISTAN  C15 1      H15 1      1.083  0.002

```

Table S3. Local axes systems of atoms.

_atom_local_axes_atom_label
 _atom_local_axes_atom0
 _atom_local_axes_ax1
 _atom_local_axes_ax2
 _atom_local_axes_atom1
 _atom_local_axes_atom2

O1	C1	XY	O1	O2	CL1	C12	ZX	CL1	C11
O2	C1	bZX	O2	H2	CL2	C16	ZX	CL2	C11
H2	O2	ZX	H2	C1	N1	C11	bZX	N1	C10
O3	C3	bZX	O3	C2	H1	N1	ZX	H1	C11
O4	C3	XY	O4	O3					
C1	O2	bXY	C1	O1	C8	C9	bXY	C8	C7
C2	O3	bZX	C2	C1	H8	C8	ZX	H8	C9
H2A	C2	ZX	H2A	O3	C9	C10	bXY	C9	C8
H2B	C2	ZX	H2B	O3	H9	C9	ZX	H9	C10
C3	O3	bXY	C3	O4	C10	C5	bXY	C10	C9
C4	C3	bZX	C4	C5	C11	C16	bXY	C11	C12
H4A	C4	ZX	H4A	C3	C12	C11	bXY	C12	C13
H4B	C4	ZX	H4B	C3	C13	C12	bXY	C13	C14
C5	C10	bXY	C5	C6	H13	C13	ZX	H13	C12
C6	C5	bXY	C6	C7	C14	C15	bXY	C14	C13
H6	C6	ZX	H6	C5	H14	C14	ZX	H14	C15
C7	C6	bXY	C7	C8	C15	C16	bXY	C15	C14
H7	C7	ZX	H7	C6	H15	C15	ZX	H15	C16
					C16	C11	bXY	C16	C15

Table S4. Statistics on Theoretical refinement.

$\sin\theta_{\max}/\lambda$ (\AA^{-1})	1.00
independent reflections	38 904
Weighting scheme for $gof=1$	$\text{Sigma}(F) = 0.092$
$R(F)$, $wR^2(I)$ (%)	0.40 , 0.80
$\Delta\rho$ min, max, rms	-0.20 , +0.22 , 0.013

R -factor and goodness of fit in resolution shells and in shells of structure factors F_{hkl} .

Shell $s < (\text{\AA}^{-2})$	$R(F)$ (%)	gof
$s < 0.464$	0.445	1.796
$s < 0.585$	0.421	1.179
$s < 0.669$	0.438	1.111
$s < 0.737$	0.410	1.000
$s < 0.794$	0.360	0.797
$s < 0.843$	0.344	0.725
$s < 0.888$	0.375	0.728
$s < 0.928$	0.355	0.688
$s < 0.965$	0.378	0.680
$s < 1.000$	0.429	0.722

Shell $F <$	number (hkl)	$R(F)$ (%)	gof
2.41	1281	5.07	0.75
4.96	1281	1.71	0.91
7.61	1283	1.00	0.89
10.54	1281	0.71	0.93
13.71	1287	0.52	0.91
17.14	1274	0.43	0.94
21.45	1285	0.35	0.98
26.96	1277	0.28	0.99
35.87	1281	0.24	1.07
420.1	1282	0.20	2.412
all	12 812	0.401	1.000

checkCIF (basic structural check) running

checkCIF/PLATON (basic structural check)

Structure factors have been supplied for datablock(s) I

THIS REPORT IS FOR GUIDANCE ONLY. IF USED AS PART OF A REVIEW PROCEDURE FOR PUBLICATION, IT SHOULD NOT REPLACE THE EXPERTISE OF AN EXPERIENCED CRYSTALLOGRAPHIC REFEREE.

No syntax errors found.
Please wait while processing

[CIF dictionary](#)
[Interpreting this report](#)

[Structure factor report](#)

Datablock: I

Bond precision:	C-C = 0.0002 Å	Wavelength=0.71073	
Cell:	a=12.3441(3)	b=0.2073(2)	c=15.3263(4)
	alpha=90	beta=95.053(2)	gamma=90
Temperature: 100 K			
	Calculated	Reported	
Volume	1521.64(7)	1521.64(7)	
Space group	P 21/n	P_21/n	
Hall group	: -P 2yn	-P_2yn	
Moiety formula	C16 H13 Cl2 N O4	C16 H13 Cl2 N O4	
Sum formula	C16 H13 Cl2 N O4	C16 H13 Cl2 N O4	
Mr	354.17	354.17	
Dx,g cm-3	1.546	1.547	
Z	4	4	
Mu (mm-1)	0.446	0.450	
F000	728.0	728.0	
F000'	729.51		
h,k,lmax	32,22,41	32,22,41	
Nref	31552	30892	
Twin,Tmax	0.911,0.953	0.929,0.959	
Twin'	0.911		
Correction method= # Reported T Limits: Twin=0.929 Tmax=0.959 AbsCorr =			
MULTI-SCAN			
Data completeness= 0.979	Theta(max)= 74.020		
R(reflections)= 0.0127(20385)	wR2(reflections)= 0.0174(30892)		
S = 0.986	Mpar= 771		

The following ALERTS were generated. Each ALERT has the format

test-name_ALERT_alert-type_alert-level.

Click on the hyperlinks for more details of the test.

Alert level C

PLAT218_ALERT_3_C Constrained U(ij) Components(s) for H2 . 6 Check

And 12 other PLAT218 Alerts

More ...

PLAT353_ALERT_3_C Long N-H (N0.07,N1.01A) N1 - H1 . 1.01 Ang.

PLAT911_ALERT_3_C Missing PCF Refl Between Thmin & STh/L= 0.600 7 Report

PLAT921_ALERT_3_C R1 in the CIF and PCF Differ by 0.0022 Check

Alert level G

PLAT002_ALERT_2_G Number of Distance or Angle Restraints on AtSite 13 Note

PLAT431_ALERT_2_G Short Inter HL..A Contact Cl1 ..O4 . 3.09 Ang.

x,-1+y,z = 1_545 Check

PLAT860_ALERT_3_G Number of Least-Squares Restraints 31 Note

PLAT912_ALERT_4_G Missing # of PCF Reflections Above 5Th/L= 0.600 655 Note

PLAT913_ALERT_3_G Missing # of Very Strong Reflections in PCF 1 Note

PLAT961_ALERT_5_G Dataset Contains no Negative Intensities Please Check

PLAT978_ALERT_2_G Number C-C Bonds with Positive Residual Density. . 9 Info

0 ALERT level A = Most likely a serious problem - resolve or explain

0 ALERT level B = A potentially serious problem, consider carefully

16 ALERT level C = Check. Ensure it is not caused by an omission or oversight